

Sub-millennial eruptive recurrence in the silicic Mangaone Subgroup tephra sequence, New Zealand, from Bayesian modelling of zircon double-dating and radiocarbon ages

Authors

Martin Danišík^{1*}, David J. Lowe², Axel K. Schmitt³, Bjarne Friedrichs³, Alan G. Hogg², Noreen J. Evans¹

¹ School of Earth and Planetary Sciences/John de Laeter Centre, Curtin University, Perth, WA 6845, Australia;

² School of Science, University of Waikato, Private Bag 3105, Hamilton 3240, New Zealand;

³ Institute of Earth Sciences, Ruprecht-Karls-Universität Heidelberg, Im Neuenheimer Feld 236, D-69120 Heidelberg, Germany.

* Corresponding author: Martin Danišík, Low-Temperature Thermochronology Facility, John de Laeter Centre, Curtin University, Perth, WA 6845, Australia, e-mail: m.danisik@curtin.edu.au; Tel. +61-(0)8-9266 2793

Final MS of article published in QSR (which is the definitive version) as follows:

Danišík, M., Lowe, D.J., Schmitt, A.K., Friedrichs, B., Hogg, A.G., Evans, N.J. 2020. Sub-millennial eruptive recurrence in the silicic Mangaone Subgroup tephra sequence, New Zealand, from Bayesian modelling of zircon double-dating and radiocarbon ages. *Quaternary Science Reviews* 246 <https://doi.org/10.1016/j.quascirev.2020.106517> (online 29 August 2020)

22 Abstract

23 Accurate dating of young (<1 Ma) volcanic eruptions has long been a challenge for modern
24 geochronology given the scarcity of datable mineral phases and low quantities of radiogenic daughter
25 products. Combined U-Th-Pb and (U-Th)/He dating of zircon (i.e. zircon double-dating, ZDD) is a
26 relatively new dating approach that offers a viable option for dating zircon-bearing volcanic and
27 pyroclastic deposits as young as ca. 3 ka, and has a great potential for application in many fields
28 within the Quaternary sciences, including volcanology, palaeoclimatology, and archaeology. In our
29 study, a stratigraphically and spatially well-defined sequence of 13 rhyodacitic to rhyolitic tephra
30 beds – the Mangaone Subgroup (MSg) – erupted from the Okataina Volcanic Centre (OVC), is used
31 as a natural laboratory to conduct a cross-validation experiment in which the ZDD eruption ages are
32 compared with published and new radiocarbon (^{14}C) eruption ages. These ZDD and ^{14}C ages are
33 then used together to underpin a Bayesian age model developed (using ChronoModel) to
34 provide new ages for the entire MSg sequence. New ZDD eruption ages of 36.1 ± 4.4 , $31.5 \pm$
35 5.2 , 30.9 ± 5.6 , 31.2 ± 4.4 ka BP for four MSg tephras (Units D, I, J, and K, respectively) are
36 statistically indistinguishable from ^{14}C -based eruption ages. These results validate the
37 feasibility of ZDD to date late Quaternary eruptions accurately. The Bayesian age sequence
38 model provides a revised eruptive geochronology for all 13 MSg tephra beds for the first time (and
39 for the stratigraphically-interbedded Taupo-volcano-derived Tahuna tephra, 38.4
40 $^{+1.7}_{-1.4}$ ka BP), and constrains the beginning of the MSg eruption period to $42.7^{+3.7}_{-3.5}$
41 ka BP (Unit A) and the end to $30.6^{+0.6}_{-1.5}$ ka BP (Unit L). Thus, the entire MSg sequence was emplaced
42 in ~12,100 years, representing an eruption frequency of one event per ~930 years on average. Our
43 study demonstrates the efficacy of ZDD to yield accurate eruption ages on pyroclastic deposits,
44 highlighting its potential for dating young (<1 Ma) magmatic and eruption events that are difficult to
45 date by other geochronological methods, and that ZDD dates can be integrated with ^{14}C ages using
46 Bayesian modelling to develop new age models for long sequences of tephra beds, in this case those
47 of the MSg tephras that were deposited during MIS 3. In addition, the U-Th zircon crystallization
data revealed distinct U-Th model age spectra for older and younger MSg tephras, providing

48 geochronological evidence for a decreasing degree of interconnectedness within the OVC magma
49 reservoir during the MSg eruption period that followed caldera collapse associated with the pre-MSg
50 Rotoiti (Rotoehu) eruption at ca. 45 ka BP.

51

52 **Keywords:** zircon double-dating; (U-Th)/He; U-Th disequilibrium; radiocarbon dating; Bayesian age
53 sequence modelling; magma dynamics; Mangaone Subgroup; tephrochronology; Okataina Volcanic
54 Centre; Taupo Volcanic Zone

55

56 **Highlights**

- 57 - Cross-validation test comparing eruption ages derived by ZDD and ^{14}C is reported;
- 58 - ZDD yields accurate eruption ages for Mangaone Subgroup, concordant with ^{14}C data;
- 59 - Bayesian modelling refines eruption ages (43–30 ka) for all MSg beds and Tahuna tephra;
- 60 - Zircon U-Th data provide insights on dynamics of magma reservoir below the OVC.

61

62 1. Introduction

63 Accurate dating of young (<1 Ma) geological materials is of paramount importance to
64 Quaternary science, yet this time interval arguably presents one of the major technical challenges for
65 modern geochronology. Young volcanic eruptions are chiefly dated by high-precision techniques
66 such as radiocarbon (^{14}C) and $^{40}\text{Ar}/^{39}\text{Ar}$ on sanidine (e.g., Mark et al., 2017; Hogg et al., 2019).
67 Combined U-Th-Pb and (U-Th)/He dating of zircon (a.k.a. zircon double-dating or ZDD; Danišík et
68 al., 2017a), with an applicability range from 1 Ma to ~3 ka (Schmitt et al., 2012; Danišík et al.,
69 2017a; Kirkland et al., 2020), is a relatively new dating method (Schmitt et al., 2006, 2010b) that
70 offers a viable option.

71 ZDD principles and analytical procedures have been summarized in detail by Danišík et al.
72 (2017a). In brief, ZDD is based on ‘dependent’ determination of two distinct ages on a single zircon
73 crystal: crystallisation ages are first determined via U-Pb or U-Th disequilibrium geochronology;
74 these ages are robust crystallization ages even at magmatic conditions (Cherniak and Watson, 2001).
75 To preserve crystal volume, high spatial resolution methods with low material consumption are used,
76 such as secondary ionisation mass spectrometry (SIMS) (Fig. 1) (Schmitt et al., 2006; Schmitt, 2007,
77 2011) or laser ablation inductively coupled plasma mass-spectrometry (LA-ICPMS) (Ito and Danišík,
78 2020). Cooling ages of U-Th-Pb dated crystals are then determined via (U-Th)/He
79 thermochronometry ($T_c < 300^\circ\text{C}$; Reiners et al., 2004). For crystals with a cooling age <1 Ma, (U-
80 Th)/He data may require correction for disequilibrium in the U and Th decay chains (Farley et al.,
81 2002). The magnitude of the disequilibrium correction depends on pre-eruptive residence time and is
82 determined on a crystal-by-crystal basis from the crystallization and cooling age pairs (Schmitt et al.,
83 2010b). Finally, disequilibrium corrected (U-Th)/He ages, which are typically determined on
84 replicate crystals per sample, are used to calculate a representative mean value for the population,
85 interpreted as the eruption age (hereafter referred to ZDD eruption age).

86 Precision on ZDD eruption ages is typically 5–12% at the 2σ level, which is relatively low
87 compared to high-precision ^{14}C or sanidine $^{40}\text{Ar}/^{39}\text{Ar}$ data, commonly reported with 2σ uncertainties

88 of <2%. Nevertheless, the ZDD has tremendous potential for Quaternary geochronology as it covers
89 the critical 1 Ma to ca. 50 ka time window, which is beyond the reach of the ^{14}C method (≤ 50 ka
90 under most circumstances; Hogg et al., 2007) and difficult to access using other techniques. In fact,
91 ZDD may often be the only tool applicable to dating intermediate to silicic calc-alkaline volcanic
92 rocks or pyroclastic deposits typical of subduction zones. These materials have been notoriously
93 challenging to date using K-Ar and $^{40}\text{Ar}/^{39}\text{Ar}$ methods due to their low potassium content and the
94 frequent absence of K-rich phases, but they commonly contain zircon. Indeed, during the past five
95 years, ZDD has been increasingly applied in tephrostratigraphy, volcanic and magmatic
96 geochronology, and occasionally even in archaeology and paleoanthropology (e.g., Coble et al., 2017;
97 Mucek et al., 2017; Molnár et al., 2018; Burgess et al., 2019; Ulusoy et al., 2019; Sisson et al., 2019;
98 Gençalioglu-Kuşcu et al., 2020).

99 Several studies report demonstrably accurate ZDD eruption ages, in agreement with
100 independent geochronological constraints obtained by dating co-genetic mineral phases or bracketing
101 units (e.g., Schmitt et al., 2010a, b; Danišik et al., 2012; Harangi et al., 2015; Ito and Danišik, 2020).
102 Moreover, ZDD has a unique built-in consistency check because the eruption age has to postdate the
103 zircon crystallization age. However, as with any geochronological method, maintaining a level of
104 scepticism about reliability of the age relevance of ZDD results is warranted, in particular when ZDD
105 ages are not entirely concordant with long accepted ages derived using more established methods
106 (e.g., Wilson and Rowland, 2016; Hopkins et al., 2017; Chesner et al., 2020). U-Th-Pb and (U-Th)/He
107 dating procedures are usually vetted against secondary reference materials (e.g., AS3 and 91500
108 zircons for U-Th-Pb and Fish Canyon zircon for (U-Th)/He); however, a suitable reference material
109 that can be used to monitor the accuracy of the coupled ZDD approach has not yet been developed.
110 Ideally, this standard would be a well characterized, widely available zircon with an accurately and
111 precisely known crystallization and eruption age of <350 ka (for the U-Th + (U-Th)/He dating
112 combination) or <1 Ma (for the U-Pb + (U-Th)/He dating combination). Secondly, verification of
113 ZDD eruption ages against independent constraints is only rarely possible in nature due to the scarcity

114 of truly co-genetic minerals or other materials in volcanic deposits that are datable by independent
115 geochronological methods. Lastly, with the exception of studies by Schmitt et al. (2012) and Danišik
116 et al. (2012), the accuracy of ZDD has not been rigorously tested. Therefore, there is a need for further
117 cross-validation studies that compare ZDD results with independent dating techniques.

118 This work describes such a cross-validation experiment in which we target a
119 stratigraphically and spatially well-defined sequence of Mangaone Subgroup tephra from New
120 Zealand's North Island (Vucetich and Pullar, 1969; Howorth, 1975). The Mangaone Subgroup
121 (MSg) tephra beds represent the products of 13 primarily rhyolitic eruption episodes at the
122 Okataina Volcanic Centre (OVC), within the central Taupo Volcanic Zone (Fig. 2), that
123 occurred between about 50 and 25 ka (Jurado-Chichay and Walker, 2000, 2001a; Smith et al.,
124 2002, 2005). This period is entirely within Marine Isotope Stage 3 (e.g., Wright et al., 1995; Wilson
125 et al., 2007; Siddall et al., 2008). Some of the MSg tephra have been extensively dated by ^{14}C
126 methods (34 published dates since 1969) and so the general timeframe of their eruptive history is
127 now established (Froggatt and Lowe, 1990; Jurado-Chichay and Walker, 2000; Shane et al., 2006;
128 Molloy et al., 2009). However, around half of the 13 beds in the sequence have never been dated
129 directly. The tephra are silicic in composition (see Section 2) and some contain zircon
130 (Charlier and Wilson, 2010). They are well exposed, regionally widespread (including in marine
131 cores), and their stratigraphic framework has been established in detail (Howorth, 1975; Jurado-
132 Chichay and Walker, 2000; Nairn, 2002; Smith et al., 2002; Shane et al., 2006; Wilson et al., 2009).
133 Cumulatively, these attributes make the MSg an excellent natural laboratory in which to test the
134 accuracy of ZDD against eruption ages derived from the ^{14}C method.

135 Accordingly, we report here ZDD eruption ages for some MSg tephra, complemented with
136 new high-precision ^{14}C ages. Our results demonstrate the capability of the ZDD approach to
137 yield accurate eruption ages. In addition to the new geochronological data, we present a new
138 Bayesian age sequence model combining both the ZDD and ^{14}C data with stratigraphic constraints,
139 and reconstruct a more robust eruptive chronology for the entire Mangaone Subgroup, the first time
such a modelling approach has been used for the sequence. In doing so, we provide new
modelled ages for the

beginning (Unit A) and end (Unit L) of the MSg tephra sequence. Finally, we assess the implications of new ZDD data for OVC magmatic dynamics.

2. Mangaone Subgroup

2.1 Volcanologic and compositional context

The Mangaone Subgroup (MSg) is a sequence of 13 silicic plinian and phreatoplinian pyroclastic deposits (tephras) that originated from the OVC (northeast part of the central Taupo Volcanic Zone) (Jurado-Chichay and Walker, 2000; Smith et al., 2002). The MSg beds are stratigraphically bracketed by (i) deposits of the underlying Rotoiti Tephra Formation (which formally comprises three members: Matahi Scoria, from basaltic fallout; the non-welded Rotoiti Ignimbrite, from rhyolitic pyroclastic flows (density currents); and the Rotoehu Ash, from rhyolitic fallout: Froggatt and Lowe, 1990) (45.2 ± 3.3 ka (2σ); Danišik et al., 2012); and (ii) the overlying Kawakawa/Oruanui tephra (25.4 ± 0.2 cal ka (2σ); Vandergoes et al., 2013). The two voluminous and widespread rhyolitic members of the Rotoiti Tephra are correlatives and are of the same age (Nairn, 1972), hence are used interchangeably in this paper as appropriate. (The Matahi Scoria is a minor component and not present in the sampling area and hence is not considered further.)

The MSg volcanic episode represents a period of intra-caldera modification in the OVC, which followed the caldera-forming Rotoiti eruption (ca. 45 ka) and preceded a period of caldera infilling and dome-building starting at ca. 21 ka (Nairn, 1989; Cole et al., 2010, 2014). Eruptions were typically relatively small- to medium-sized (non-consolidated volumes: 0.4–19.9 km³; minimum total bulk volume: 80.7 km³; Table 1), short-lived (<12 h), and closely spaced plinian-type, resulting in extensive pumice-rich tephra beds (Jurado-Chichay and Walker, 2000, 2001a, b; Smith et al., 2005). The MSg tephras are typically separated by paleosols, usually thin, and because of their widespread occurrence, the tephras provide useful stratigraphic marker horizons for the central and northern North Island of New Zealand (Pullar et al., 1973; Hogg and McCraw, 1983; McGlone et al., 1984; Molloy et al., 2009; Hopkins et al., 2017) and offshore including the Pacific Ocean (Fig. 2)

166 (Houghton et al., 1992; Pillans and Wright, 1992; Wright et al., 1995; Shane et al., 2006; Wilson,
167 2007). Compositions of MSg tephra range from rhyodacitic to rhyolitic (68–75.5 wt% SiO₂; Smith
168 et al., 2002, 2005) and at least two contain zircon (Charlier and Wilson, 2010), providing an
169 opportunity to apply ZDD.

170

171 ***2.2 Nomenclature and stratigraphy***

172 Different nomenclature has been used interchangeably in the literature to describe the MSg
173 tephra beds, which may be confusing to readers unfamiliar with New Zealand tephrostratigraphy. We
174 therefore provide a short review of MSg terminology and stratigraphy as they are currently
175 understood.

176 The MSg sequence was first referred to as the ‘Mangaoni Lapilli Formation’ by Vucetich and
177 Pullar (1969). The authors used the term to describe a distinct package of shower-bedded pumice
178 lapilli and blocks and ash beds, bracketed by the Rotoehu Ash (below) and Oruanui Formation
179 (above). Five deposits were recognized (units *a–e*) within the formation (Vucetich and Pullar, 1969).
180 The name of the sequence was changed to ‘Mangaone Subgroup’, as proposed by Howorth (1981),
181 and later formalized by Froggatt and Lowe (1990) (the use of ‘Mangaone’ rather than ‘Mangaoni’
182 by Howorth in 1975 corrected a spelling error on a topographic map). The MSg tephra beds were
183 defined as originating from the OVC (Froggatt and Lowe, 1990). Cole et al. (2010, 2014)
184 employed the alternative term ‘Mangaone Pyroclastic Subgroup’. A detailed stratigraphy of the
185 sequence was first constructed by Howorth (1975), who described eight tephra formations and
186 defined them using local geographic names that have since been widely accepted. In ascending
187 stratigraphic order, these formations are Ngamotu, Tahuna, Maketu, Te Mahoe, Hauparu,
188 Mangaone, Awakeri, and Omataroa (Table 1). Note that the subgroup’s collective name
189 (Mangaone) is also used as the name of one of the constituent tephra formations.

190 The MSg stratigraphy was later revised by Jurado-Chichay and Walker (2000) and Smith et
191 al. (2002) who described 12 and 14 tephra deposits, respectively, and named these with letters (Units

192 A–L; Jurado-Chichay and Walker, 2000) or a combination of letters and local names (Smith et al.,
193 2002) (Table 1). Smith and Shane (2002) demonstrated that the Tahuna tephra did not erupt from the
194 OVC and therefore should not be a member of the Mangaone Subgroup (although it is present in the
195 MSg sequence at many sites). Further changes to the nomenclature have been made by Smith et al.
196 (2005) who subdivided the MSg based on age and composition into ‘Old MSg’ (Units A-G; ~40–35
197 ka; low-SiO₂ rhyodacite) and ‘Young MSg’ (Units H-L; ~35–31.5 ka; high-SiO₂ rhyolite) episodes,
198 and by Wilson et al. (2009) who introduced Units C1 and C2 as a compromise between Unit C *sensu*
199 Jurado-Chichay and Walker (2000) and Pupuwharau and Pongakawa tephras *sensu* Smith et al.
200 (2002) (Table 1).

201 The name ‘Kawerau Ignimbrite’ has been applied to the most voluminous and extensive of
202 the MSg eruptives, Unit I (Mangaone tephra), the eruption of which may have been accompanied by
203 partial caldera collapse (Cole et al., 2010, 2014). These authors indicate that this non-welded
204 ignimbrite is associated geochemically with the younger of the two MSg magma types noted above
205 (Smith et al., 2002). The term ‘Kawerau’ has not been widely adopted, partly because of confusion
206 regarding its age when first described, and partly because the ignimbrite had already been defined as
207 the ‘upper Mangaone member’ of the Mangaone Tephra Formation by Howorth (1975).

208 In this study we followed the latest version of stratigraphy after Wilson et al. (2009) and use
209 a ‘hybrid’ nomenclature combining the systems of Jurado-Chichay and Walker (2000) and Smith et
210 al. (2002) as presented in Table 1.

211

212 **2.3 Previous geochronology**

213 Seven of the MSg tephras have been previously dated by ¹⁴C methods (see the summary of
214 ¹⁴C data in Table 2 and Fig. 3). Preferred eruption ages and age precision for some tephras vary
215 significantly, depending on data treatment. For example, 17 ¹⁴C ages ranging between 26.2 ± 0.4 and
216 40.1 ± 2.1 cal ka BP (1σ) have been obtained for different materials from Unit I (Mangaone) (Vucetich
217 and Pullar, 1969; Pullar and Heine, 1971; Nairn, 1981; McGlone et al., 1984; Jurado-Chichay and

218 Walker, 2000). Representative eruption ages preferred by different authors based on the same dataset
219 vary from 31.6 ± 0.4 to 33.0 ± 3.7 cal ka BP (1σ) depending on data selection preference (Jurado-
220 Chichay and Walker, 2000; Shane et al., 2006). As noted by Froggatt and Lowe (1990), the
221 assumption of high quality in the ^{14}C data is not always warranted and care needs to be taken when
222 selecting data for interpretation. Similarly, McGlone et al. (1984) reported that radiocarbon ages
223 obtained on MSg tephras within peat at a site in Gisborne “do not give a conclusive indication of
224 [their] age [but] collectively they suggest that the site is between 30,000 and 40,000 years old” (p.
225 333).

226 To make the available data comparable and consistent with international standardization and
227 nomenclature, we have calibrated conventional ^{14}C ages (in ^{14}C yr BP) to calendar years (cal yr BP
228 or cal ka BP) in the OxCal 4.3 software (Bronk Ramsey, 2009) using the SHCal13 calibration curves
229 (Hogg et al., 2013) (Table 2). The ^{14}C ages from, or relevant to, the MSg that we consider reliable
230 range from 38.9 ± 0.5 (Tahuna Tephra; in Loame et al., 2019) to 30.7 ± 0.2 cal ka BP (1σ) (Unit L;
231 Jurado-Chichay and Walker, 2000).

232 As noted earlier, around half of the MSg tephras have never been directly dated by radiometric
233 methods and their ages have instead been inferred based on stratigraphic relationship and assumptions
234 relating to the duration of paleosol formation (the amount of time it took for soil horizons to be
235 developed prior to burial by new eruptives). Neither of the two stratigraphically oldest MSg tephras,
236 Unit A and Unit B (Ngamotu), has been dated directly. Consequently, the beginning of the MSg
237 eruptive phase was only indirectly estimated at ~52–43 ka based on field observations (Jurado-
238 Chichay and Walker, 2000) made in conjunction with the widely varying estimates for the eruption
239 age of the underlying Rotoiti eruptives (including the Rotoehu Ash) (Froggatt and Lowe, 1990). The
240 Rotoiti/Rotoehu deposits have been very difficult to constrain chronologically, and ages have ranged
241 from ~40 ka to 70 ka (e.g., Thompson, 1968; Grant-Taylor and Rafter, 1971; Berryman, 1992; Lowe
242 and Hogg, 1995; Lian and Shane, 2000; Santos et al., 2001; Shane and Sandiford, 2003; Wilson et
243 al., 2007; Flude and Storey, 2016). In our study, we adopt the eruption age of 45.2 ± 3.3 ka (2σ) for

the Rotoiti Tephra Formation (Danišík et al., 2012) and consider it to be the maximum age limit for the MSg tephra beds. This age was derived by ZDD and evidence supporting it includes (but is not limited to) optimum ^{14}C data (i.e., stratigraphically well-constrained samples and high-level laboratory pre-treatment) (Santos et al., 2001; Danišík et al., 2012), $^{40}\text{Ar}/^{39}\text{Ar}$ data on K-feldspar and biotite (Flude and Storey, 2016), U-Th zircon crystallization ages (Charlier et al., 2003; Charlier and Wilson, 2010; Rubin et al., 2016), as well as palynological, magnetostratigraphic, and sedimentation-rate-based ages from lake sediments and deep-sea cores (Wright et al., 1995; Shane and Sandiford, 2003; Newnham et al., 2004; Shane et al., 2006; Molloy et al., 2009; Nilsson et al., 2011; Peti and Augustinus, 2019).

Another geochronological approach applied to the MSg tephras is optical luminescence dating of paleosols beneath the Tahuna tephra by Lian and Shane (2000), who reported ages of 30 ± 2 and 34 ± 3 ka. These ages, however, are younger than the ^{14}C ages measured on the Tahuna tephra (37.5 ± 0.7 and 38.5 ± 0.6 ka) by Molloy et al. (2009) and therefore are not considered further. Finally, Charlier and Wilson (2010) reported zircon U-Th crystallization ages of $50^{+11}_{-10} - 395^{+\infty}_{-110}$ ka (weighted average: 81 ± 11 ka (95% conf. interval); $n=42$; MSWD=6.4) and $20^{+11}_{-10} - 320^{+250}_{-71}$ ka (weighted average: 51.7 ± 5.9 ka (95% conf. interval); $n=54$; MSWD=3.6) for Unit B (Ngamotu) and Unit I (Mangaone), respectively. The youngest statistically meaningful populations in the age spectra may provide a coarse estimate of the maximum limit for eruption age of these tephras.

262

263 ***2.4 Stratigraphy of sample sites***

Samples of Unit I (Mangaone), Unit J (Awakeri), and Unit K (Omataroa) were collected from the type section for Unit I (Mangaone) tephra in the Bowditch Quarry on State Highway 2 ($\text{S}38^{\circ}01'21.6''$ $\text{E}176^{\circ}43'18.2''$), designated by both Howorth (1975, p. 696) and Jurado-Chichay and Walker (2000, p. 326). Here, the exposed sequence consists of (from bottom to top; Fig. 4): paleosol on Unit F (Hauparu); Unit I (Mangaone), a ~5 m thick deposit of massive, weakly-bedded, inversely-graded pumice lapilli and blocks, which is further subdivided into a lower unit (medium-coarse

270 lapilli), middle unit (coarse lapilli and blocks) that we sampled for pumice clasts (sample NZ18-3;
271 Fig. 4A), and an upper pyroclastic flow unit (ash and pumice lapilli) which contains carbonized logs
272 that we sampled for ^{14}C dating (sample BDQ-1; Fig. 4A,B); Unit J (Awakeri) comprising a ~50-cm-
273 thick pumice fall deposit with <1 cm pumice lapilli and dark lithics fining upward. Here we collected
274 a sample (NZ18-2) of coarser pumice from the base of the formation (Fig. 4C); Unit K (Omataroa)
275 comprising a >4 m thick, mostly coarse pumice fall deposit with pumice clasts <5 cm, which we
276 sampled ~20 cm above the lower contact (sample NZ18-1; Fig. 4C); and Kawakawa tephra capping
277 the Mangaone Subgroup sequence.

278 Samples of Unit F (Hauparu) and Unit D (Maketu) were collected from a reference site
279 exposed on Little Waihi Road site (S37°45'39.7'' E176°28'20.0'') and described in Briggs et al.
280 (2006, p. 23); type locations for both units are nearby (Jurado-Chichay and Walker, 2000, p. 326).
281 The sequence comprises (from bottom to top; Fig. 4D): Rotoehu Ash (over Rotoiti Ignimbrite); a
282 ~150 cm thick prominent brown paleosol; a distinct, thin (~5 cm thick) white ash layer (possibly
283 Unit C2 (Pongakawa tephra); Briggs et al., 2006); Unit D (Maketu), consisting of a ~1.5 m thick
284 deposit with normally graded, pink-coloured coarse pumice lapilli (our sample NZ18-5; Fig. 4D) and
285 a weak paleosol; Unit F (Hauparu), comprising >2 m thick, coarse plinian-fall deposits containing up
286 to ~5 cm large pumice clasts (our sample NZ18-4; Fig. 4D).

287

288 **3. Methods**

289 ***3.1 ZDD – sample preparation, dating procedure***

290 Prior to zircon separation, ~200 g of pumice clasts from each sample were submitted to
291 Labwest Minerals Analysis Pty Ltd (Perth) for trace element analysis by solution ICPMS in order to
292 determine the whole rock Th and U abundances required for ZDD age calculation. The samples were
293 pulverized and 100 g of material was microwave digested using a proprietary method in a mixture of
294 HF, HCl, and HNO₃ under high pressure (~20 bar) and temperature (~180°C) in sealed Teflon

295 pressure vessels. The solutions were analysed for U and Th by external calibration on a Perking Elmer
296 NexION 300Q ICPMS.

297 The remaining aliquot of the sample was processed for zircon. Zircon was separated from the
298 samples at the John de Laeter Centre (JdLC) at Curtin University following a standard work-flow for
299 heavy mineral separation with some modification: samples were disaggregated to <400 μm fraction
300 using SelFrag disaggregation. This approach requires that samples be submerged in water, so pumice
301 that floated was soaked in water (usually for one week) until it sank. Heavy minerals were pre-
302 concentrated using a Jasper Canyon Research zircon concentrating table. The heavy fractions were
303 dried and processed through heavy liquids using lithium polytungstates (LST; specific gravity =
304 ~ 2.85) and magnetic separation. The heavy non-magnetic fraction was then handpicked for zircon
305 under a stereomicroscope. Finally, zircon crystals were rinsed in cold 48% HF for 3 min to remove
306 adherent glass.

307 Zircon crystals were embedded in indium (In) metal with unpolished crystal faces exposed at
308 the surface. The surface of the mount was levelled and coated with a conductive layer of gold, and
309 crystal rims were dated by U-Th disequilibrium methods with a CAMECA ims 1280-HR (SIMS) at
310 the HIP Laboratory at Heidelberg University, Germany, following the protocols for dynamic multi-
311 collection analysis described in Schmitt et al. (2017) and Friedrichs et al. (2020). ThO^+/UO^+ relative
312 sensitivities were calibrated on 91500 (Wiedenbeck et al., 1995) and AS3 (Paces and Miller, 1993)
313 zircon crystals, used as primary and secondary calibration standards, respectively. The weighted
314 average of $^{230}\text{Th}/^{238}\text{U}$ values obtained on AS3 analyses bracketing blocks of the unknowns is $1.005 \pm$
315 0.005 (1σ ; $\text{MSWD}=0.93$; $n=49$), consistent with secular equilibrium of AS3. The dimension of
316 elliptical craters sputtered on the crystal rims with a ~ 40 μm wide ion beam were ~ 40 (length) \times 25
317 (width) \times 5 μm (depth), preserving >98% of the crystal volume for subsequent (U-Th)/He analysis
318 (Fig. 1). Zircon U-Th model ages were calculated as two-point isochrons regressed through measured
319 $^{238}\text{U}/^{230}\text{Th}$ values and whole rock Th/U composition that was assumed as representative for the melt
320 composition.

321 After the SIMS analysis, mounts were wiped with methanol to remove the gold coating, and
322 zircon crystals were plucked out of the In ahead of (U-Th)/He dating in the JdLC Low-Temperature
323 Thermochronology Facility (Curtin University) following the procedures described in Danišík et al.
324 (2012; 2017a). The crystals were photographed, measured for physical dimensions, transferred and
325 packed into niobium (Nb) microtubes and loaded into an Alphachron II instrument for He extraction.
326 ^4He together with other gases were extracted at $\sim 1,250^\circ\text{C}$ under ultra-high vacuum using a diode
327 laser, cleaned on Ti-Zr getters, and spiked with 99.9% pure ^3He gas. The volume of ^4He was measured
328 by isotope dilution on a QMG 220 M1 Pfeiffer Prisma Plus mass spectrometer. A “re-extract” was
329 run after each analysis to verify complete outgassing of the crystal. Helium gas signals were corrected
330 for blank, determined by analysing empty Nb microtubes interspersed between the unknowns using
331 the same gas extraction procedure. After the He measurements, Nb microtubes containing the crystals
332 were retrieved from the Alphachron, spiked with ^{235}U and ^{230}Th , and dissolved in Parr acid digestions
333 vessels in two cycles of HF, HNO_3 (cycle 1), and HCl acids (cycle 2) following the procedures
334 described in Evans et al. (2005). Sample, blank, and spiked standard solutions were then diluted by
335 Milli-Q water and analysed by isotope dilution for ^{238}U and ^{232}Th , and by external calibration for
336 ^{147}Sm on an Element XRTM High Resolution ICP-MS. The total analytical uncertainty (TAU) was
337 calculated as a square root of sum of squares of uncertainty on He and weighted uncertainties on U,
338 Th, and Sm measurements. The zircon (U-Th)/He ages were corrected for alpha ejection (Ft-
339 correction) after Farley et al. (1996), whereby homogenous distributions of U, Th, and Sm were
340 assumed for the crystals. The accuracy of the zircon (U-Th)/He dating procedure was monitored by
341 replicate analyses of internal standard Fish Canyon Tuff zircon where crystals measured over the
342 course of this study yielded a mean (U-Th)/He age of 28.5 ± 0.3 Ma (1σ ; MSWD=1.03; n=13), in
343 excellent agreement with the reference (U-Th)/He age of 28.3 ± 1.3 Ma (Reiners, 2005).

344 The Ft-corrected (U-Th)/He ages were then corrected for U-series disequilibrium and pre-
345 eruptive crystal residence time (Farley et al., 2002) using MCHecalc software (Schmitt et al., 2010).
346 In addition to the Ft-corrected (U-Th)/He ages and U-Th crystallization ages (with their associated

uncertainties), the software also requires D_{230} and D_{231} parameters which describe zircon-melt fractionation of Th and Pa relative to U. Calculation of D_{230} (Farley et al. 2002) was made by dividing zircon Th/U values by whole-rock Th/U, whereby we assume that the magma was in secular equilibrium and that the measured whole-rock values are representative for the magma from which the zircons originated. For D_{231} a value of 3.3 was adopted based on an average of published Pa/U zircon-rhyolite melt partition coefficient values (Schmitt, 2007, 2011; Sakata et al., 2017). Disequilibrium corrected (U-Th)/He ages (7 to 9 replicates per sample) were then used to calculate mean value, which is interpreted as the representative eruption age of each sample (and termed ZDD eruption age). This was done by applying two different approaches. In the first, traditionally-used ‘frequentist approach’, the error-weighted mean with 95% confidence intervals were calculated using Isoplot v.4.15 Excel add-in (Ludwig, 2012). In the second (novel) ‘Bayesian approach’, we applied a Bayesian probability model to predict posterior mean values and their 95% high density intervals (HDI) using an approach described in Mucek et al. (submitted). In addition, we also applied Bayesian analysis for comparing two groups to test whether there is a statistically significant difference between the ZDD ages obtained on different tephtras.

To enable direct comparison of ZDD eruption ages with ^{14}C ages, conventional ZDD eruption ages were converted to calendar kiloyears before present (ka BP), where present = 1950 CE.

365

3.2 ^{14}C dating procedure

Two aliquots of charcoal sample BDQ-1 from Unit I (Mangaone) tephra were analysed by liquid scintillation spectrometry at the Waikato Radiocarbon Dating Laboratory (New Zealand) following the methods described in Hogg et al. (2007). The analysis utilized acid–base–acid pre-treatment. The $\delta^{13}\text{C}$ values were measured as $-21.2 \pm 0.2\text{‰}$. Background blank correction (equivalent to an apparent age of 54.1 ka BP) was achieved by ^{14}C analysis of MIS 5 (~120 ka) wood (Hogg et al., 2007). The resulting conventional ^{14}C age (^{14}C yr BP) was calibrated to calendar years (cal yr BP) by OxCal 4.3 (Bronk Ramsey, 2009) using the SHCal13 calibration curves (Hogg et al., 2013).

373 Previously published ^{14}C ages were calibrated to calendar years by the same procedure to enable
374 comparison with our new ZDD and ^{14}C results.

375

376 ***3.3 Age sequence modelling using Bayesian inference***

377 To reconstruct a robust eruptive chronology for the MSg sequence, a Bayesian ‘target event
378 date model’ (Lanos and Philippe, 2017, 2018) incorporating ZDD and ^{14}C geochronological data, as
379 well as stratigraphic information, was developed in ChronoModel v. 2.0 software (Lanos and
380 Dufresne, 2019). This software was originally designed for archaeological purposes, to estimate the
381 date of events by combining numerical (absolute) dates obtained (often by different methods) on
382 archaeological artefacts, as well as relative dates inferred from their stratigraphic position. These data
383 can be used as prior information for the modelling, which is based on a hierarchical Bayesian
384 statistical approach and utilizes Markov chain Monte Carlo (MCMC) numerical techniques to
385 estimate the dates of target events and their uncertainties. One of the major advantages of the target
386 event date model (Lanos and Philippe, 2017, 2018) over other Bayesian chronological modelling
387 packages such as OxCal and BCal is in the robustness of predicted dates that yield a less precise but
388 more accurate reflection of the chronology (Lanos and Philippe, 2018).

389 The schematic structure of the MSg tephra model can be found in Supplementary Figure S1,
390 and input data are listed in Supplementary Table S1. In the model, tephtras were defined as separate
391 events characterized by ZDD and/or ^{14}C data (i.e., ages and 1σ uncertainties) from this study or
392 published literature. Tephtras with no available radiometric data were loosely constrained as
393 uninformative dates, ranging from the oldest age of the underlying unit to youngest age of the
394 overlying unit. The relative chronology of the events was constrained based on stratigraphic
395 superpositioning. Maximum and minimum age limits of the whole sequence were constrained by the
396 eruption ages of the Rotoiti Tephra and Earthquake Flat Tephra formations (45.2 ± 1.65 and $45.2 \pm$
397 1.45 ka (1σ), respectively; Danišik et al., 2012) and Oruanui/Kawakawa tephra (25.4 ± 0.1 cal ka BP;
398 Vandergoes et al., 2013), bracketing the MSg sequence. We ran three MCMC sampling chains

399 consisting of 1,000 burn-in, 10,000 adaptation and 100,000 acquisition iterations; thinning rate was
400 set to 10. The model calculates posterior distributions for event dates that are described by a range of
401 parameters; for simplicity we will refer to mode of the posterior distribution (MAP or maximum *a*
402 *posterior* probability) and 95% highest posterior density (HPD) region estimates (i.e., an analogue to
403 2σ uncertainty range in frequentist statistics) as representative values for the posterior event dates.

405 **4. Results**

406 **4.1 U-Th crystallization ages**

407 In total, four samples were dated by ZDD; one sample NZ18-4 (Unit F, Hauparu) yielded only
408 a few small zircon crystals ($<40\ \mu\text{m}$ in diameter), of inadequate size for ZDD. Analytical results are
409 summarized in Supplementary Table S2. Analyses of all crystal surfaces revealed ^{230}Th deficits;
410 $(^{230}\text{Th})/(^{238}\text{U})$ values (parentheses indicate activities) are below unity, with data plotting to the right
411 of the equiline (Fig. 5), suggesting a crystallization age $\ll 350\ \text{ka}$ for all 59 dated crystals. U-Th
412 model ages defined by zircon and whole rock compositions range from ca. 25 ± 8 to $113 \pm 39\ \text{ka}$ (1σ).
413 U-Th age spectra (Fig. 6) for all four samples are unimodal with mean values of ca. 40 ka for the
414 stratigraphically higher samples (Unit I (Mangaone), Unit J (Awakeri), Unit K (Omataroa)) and ca.
415 60 ka for the stratigraphically lowest sample, Unit D (Maketu).

417 **4.2 (U-Th)/He ages**

418 Seven to nine SIMS-dated zircon crystals per sample were dated by the (U-Th)/He method.
419 Alpha-ejection corrected (U-Th)/He ages are younger than their corresponding U-Th ages for all 33
420 double-dated crystals (Table 3; Supplementary Table S3). One crystal (NZ18-5-17) had an extremely
421 large analytical uncertainty (160%; 1σ) due to the low He content and was rejected from further
422 evaluation. The remaining Ft-corrected (U-Th)/He ages corrected for disequilibrium yield weighted
423 mean ages (arranged in stratigraphical order from bottom to top) of: Unit D (Maketu) 36.1 ± 4.4
424 ka BP (95% conf.; MSWD = 1.5; $n = 7$); Unit I (Mangaone), 31.5 ± 5.2 ka BP (MSWD = 1.8; $n =$
7);

Unit J (Awakeri) 30.9 ± 5.6 ka BP (MSWD = 1.13; n = 8); and Unit K (Omataroa) 31.2 ± 4.4 ka BP (MSWD = 1.04; n = 9) (Fig. 6; Table 3). The weighted mean ages and their uncertainties are almost identical to the posterior mean values and 95% HDIs determined by Bayesian inference (Fig. 7; Table 3). Individual grain ages are reproducible within analytical uncertainty (Figs. 6, 7) and the MSWD values (~ 1 – 1.8) are in the acceptable range of a reduced chi-squared test for sample sizes of 7–9 (Spencer et al., 2016). Therefore, the data for each sample are interpreted to represent a single population and the weighted mean values are our best estimates of ZDD eruption ages.

Due to the large age uncertainties, the relationship between the ZDD ages and relative stratigraphic position of the tephras that were sampled is not very clear. Bayesian inference revealed that only the sample from Unit D (Maketu) with the lowest position in the stratigraphic sequence and the oldest ZDD age is statistically different from the upper three tephras, which yielded statistically indistinguishable ZDD ages (Fig. 7). The statistical overlap in ages is not surprising given that paleosols formed on each unit are thin and weakly developed (Jurado-Chichay and Walker, 2000). These periods of volcanic quiescence (paraconformities mark the boundary between the buried paleosol top and overlying tephra) likely correspond to a few decades to centuries (Jurado-Chichay and Walker, 2000), through to a maximum few thousand years based on clay content and thickness (Hodder et al., 1990; Lowe and Percival, 1993; Lowe and Hogg, 1995).

4.3 ^{14}C ages

Two aliquots of sample BDQ-1 (Unit I (Mangaone)) yielded conventional ^{14}C ages of $26,846 \pm 117$ and $26,892 \pm 117$ yr BP (1σ), calibrated to 2σ probability age ranges of 30,752–31,150 and 30,777–31,171 cal yr BP, respectively (Table 2; Supplementary Table S4). These ages are in good agreement with high-precision ^{14}C 2σ age ranges of 31,095–32,357 and 31,456–33,003 cal yr BP on charcoal reported for the same tephra by Jurado-Chichay and Walker (2000) (Table 2).

Therefore, we combined these four ages using the R_combine function in OxCal 4.3 and calculated

a pooled 2σ age range of 30,902–31,247 cal yr BP (2σ age range), which is considered our optimum

estimate for Unit I (Mangaone). We did not include other published ^{14}C ages because of their lower precision or problems with sample material as discussed in Froggatt and Lowe (1990) and Jurado-Chichay and Walker (2000).

5. Interpretation and discussion

5.1 Comparison of ZDD eruption ages and ^{14}C ages

The new ZDD eruption ages are in excellent agreement with the corresponding ^{14}C ages. Both methods yielded statistically indistinguishable ages, fully overlapping within 2σ uncertainty: for Unit D (Maketu), the ZDD age of 36.1 ± 4.4 ka BP overlaps with the ^{14}C 2σ age range of 35.2–36.6 cal ka BP (Molloy et al., 2009). For Unit I (Mangaone), the ZDD age of 31.5 ± 5.2 ka BP is concordant with the preferred optimum ^{14}C 2σ age range of 30.9–31.2 cal ka BP based on pooled high-precision ^{14}C data obtained on charcoal from Jurado-Chichay (2000) and our study. The ZDD age of 30.9 ± 5.6 ka BP is the first radiometric age reported for Unit J (Awakeri), and is concordant with the bracketing ^{14}C 2σ age ranges of 30.9–31.2 and 31.2–33.7 cal ka BP from underlying Unit I (Mangaone) and overlying Unit K (Omataroa), respectively. The 31.2–33.7 cal ka BP 2σ age range for Unit K (Omataroa) overlaps with the ZDD age of 31.2 ± 4.4 ka. The concordance of ages from two independent radiometric dating methods suggests that both methods are accurate because they are dating the same eruption event (as determined by stratigraphy). Accepting the optimum ^{14}C ages as the ‘gold standard’ for eruption age estimation, the excellent agreement of ^{14}C ages and ZDD ages demonstrates the accuracy of eruption ages derived by ZDD.

The precision of the ZDD eruption ages (i.e., 12–18% age uncertainties at 2σ) is lower than typical ZDD uncertainties of 5–12% (2σ) reported in literature. The precision of ZDD eruption ages is usually related to (over-)dispersion of single crystal (U-Th)/He ages associated with complexities inherent in (U-Th)/He dating systematics (Vermeesch, 2010; Danišik et al., 2017b), and not to the analytical uncertainty of actual measurements. In the case of the data for the MSg tephra sequence generated in this work, the dispersion of single crystal (U-Th)/He ages is not large, with MSWD

477 values close to unity. Instead, the major source of ZDD uncertainty stems from the low He content
478 (and hence large uncertainty associated with He measurements; Table 3), which is related to the
479 young cooling age of the crystals, and to an unusually low U content (ca. 100 ppm on average),
480 significantly lower than typical U concentrations in zircon (300-600 ppm; e.g., Wagner and Van den
481 haute, 1992).

482 Although the ZDD ages are accurate, precision could likely have been improved by increasing
483 the number of dated crystals. In this study we aimed for 7 to 9 crystals to be double-dated per sample.
484 While we acknowledge that some studies dated up to ~20 replicates per sample in order to achieve
485 high precision ZDD eruption ages (e.g., Danišík et al., 2012; Coble et al., 2017), we considered 7–9
486 crystals an adequate number to obtain the desired precision of 5–12% (2σ) following the example of
487 some other studies (e.g., Schmitt et al., 2011; Molnár et al., 2018). To test whether a larger number
488 of grains per sample would improve precision, we combined the disequilibrium corrected (U-Th)/He
489 ages of samples NZ18-1, NZ18-2, and NZ18-3 from Unit I (Mangaone), J (Awakeri), K (Omataroa),
490 i.e., samples with overlapping eruption ages. The resulting weighted mean values of 31.0 ± 3.4 ka
491 (NZ18-1 and NZ18-2 combined; $n = 17$; MSWD = 1.01) and 31.2 ± 2.9 ka (all 3 samples combined;
492 $n = 24$; MSWD = 1.17) have an uncertainty of 11% and 9.2 %, respectively, which are within our
493 desired precision range for the ZDD approach. These results also show that analysing ~15 crystals of
494 low-U MSg zircon per sample should suffice to generate reasonably precise ages.

495 The new data demonstrate the capability of ZDD to yield accurate eruption ages. Nevertheless,
496 it should be noted that ZDD accuracy can be affected by several factors. These include the presence
497 of mineral or fluid inclusions potentially leading to older than expected (U-Th)/He ages (e.g., Danišík
498 et al., 2017b), incomplete resetting of xenocrysts (e.g., Blondes et al., 2007; Ulusoy et al., 2019),
499 heterogeneous distribution of parent nuclides impacting the alpha ejection correction (Hourigan et
500 al., 2005; Danišík et al., 2017b), and simplified assumptions about duration of zircon crystallization
501 and parental melt composition potentially affecting the magnitude of disequilibrium correction
502 (Schmitt, 2011; Storm et al., 2012; Boehnke et al., 2013; Danišík et al., 2017a). In our study, we

503 followed a routine, well-established workflow and used optical microscopy to select euhedral,
504 inclusion free crystals. However, no special effort was made to characterize crystal interiors for U-
505 Th zonation or complexity of crystallization history. Although this “rudimentary” approach arguably
506 yielded accurate ZDD eruption ages as demonstrated by the concordance with ^{14}C data, we emphasize
507 that more detailed crystal characterization may be critical in other ZDD studies.

508

509 ***5.2 Eruption age sequence modelling using Bayesian inference***

510 In order to integrate and utilize all the information from the available dataset and well-defined
511 stratigraphy, we built a Bayesian age sequence model using ChronoModel v. 2.0 software (Lanos and
512 Dufresne, 2019). In doing so we aimed to: (i) develop a robust, comprehensive and up-to-date
513 eruptive chronology for the MSg tephra beds; (ii) realistically estimate the ages and quantify age
514 uncertainties for those units that have not been directly radiometrically dated; and (iii) test the
515 sensitivity of the Bayesian model to different types of input data.

516 The schematic structure of the model was described in Section 3.3. In brief, a sequence of 14
517 events is defined, representing 13 MSg tephra and Tahuna tephra in stratigraphic order as defined in
518 Smith et al. (2005) and Wilson et al. (2009) (Table 1). The sequence is bracketed from the bottom by
519 the Rotoiti and Earthquake Flat events with assigned eruption ages of 45.2 ± 1.65 and 45.2 ± 1.45 ka
520 BP (Danišík et al., 2012), respectively, and by the Oruanui/Kawakawa event at the top with an
521 eruption age of 25.4 ± 0.2 cal ka BP (Vandergoes et al., 2013) (Supplementary Figure S1). Three
522 models with different input parameters were constrained as follows (Supplementary Table S1): Model
523 1 took into account only ^{14}C data that we considered of the highest quality available for each tephra
524 as specified in Table 2. These data were complemented in Model 2 with ZDD data. In Model 3 we
525 considered all ^{14}C data, regardless of quality, and ZDD data.

526 Results presented in Figure 8 show that the posterior eruption ages and uncertainties predicted
527 by the three models are almost identical. Only a subtle difference in age uncertainty of <0.5 ka is
528 present in model ages for Units I (Mangaone), J (Awakeri), and K (Omataroa), with Model 3

529 predicting the lowest, and Model 2 the highest, uncertainties (Fig. 8). The excellent overall similarity
530 of the posterior eruption ages predicted by the three models demonstrates that our modelling approach
531 based on hierarchical Bayesian inference is not significantly affected by the presence of outliers and
532 offers a robust means to estimate the chronology of eruption events based on multiple
533 geochronological data combined with a priori information from stratigraphic
534 superpositioning.

535 For interpretation purposes, we will adopt the posterior distributions of Model 2, based on the
536 highest quality ^{14}C and ZDD data, as our best estimates for eruption ages for the MSg tephras (Fig.
537 9). These results constrain the duration of MSg activity between $42.7^{+3.7}_{-3.5}$ and $30.6^{+0.6}_{-1.5}$ ka BP (MAP
538 \pm 95% HPD) based on posterior distributions for Unit A and Unit L, respectively. The beginning of
539 MSg activity is of particular importance here because this age was only indirectly estimated based on
540 the age of underlying Rotoiti/Rotoehu deposits, which for several decades had been considered to be
541 in the 64–61 ka range (Wilson et al., 1992, 2007). Nevertheless, some authors estimated the onset of
542 MSg activity to have taken place ~44–43 ka (no uncertainties provided; Jurado-Chichay and Walker,
543 2000; Wilson et al., 2009; Leonard et al., 2010). Our modelled onset age (~43 ka) implies that several
544 volcanic deposits that occur in stratigraphic juxtapositions between the Rotoiti/Rotoehu and MSg
545 tephras are younger than previously considered (e.g., six un-named eruptives from Taupo caldera and
546 Forest Rd dome from Maroa caldera, reported in Wilson et al., 2009, and the Otake, Waihora, and
547 Tihoi tephras, reported in Vucetich and Howorth, 1976; Froggatt and Lowe, 1990; Wilson et al.,
548 2009). Our results also suggest a much shorter period of quiescence between the Rotoiti/Rotoehu and
549 MSg events, lasting no more than a few thousand years, which has implications for calculation of
550 magma eruption rate for the OVC. Finally, in addition to Unit A ($42.7^{+3.7}_{-3.5}$ ka BP), based on the new
551 data herein, we propose the following ages and uncertainties for previously undated MSg tephras:
552 Unit B (Ngamotu) – $39.6^{+4.5}_{-1.9}$; Unit C1 (Pupuwarau) – $37.7^{+1.5}_{-1.4}$; Unit C2 (Pongakawa) – $36.6^{+1.6}_{-1.0}$;
553 Unit G – $33.8^{+1.7}_{-2.0}$; and Unit H – $31.8^{+2.6}_{-0.8}$ ka BP (MAP \pm 95% HPD).

554

555 *5.3 Implications for magmatic evolution of the Okataina Volcanic Centre*

556 In addition to eruptive chronology, ZDD may provide insights into the dynamics of magmatic
557 systems via direct provision of zircon U-Th crystallization ages (Schmitt, 2011). Although our dataset
558 for the four dated tephras is of smaller size ($n = 59$) and lacks information on trace element or isotopic
559 composition of zircon, the U-Th age spectra allow us to identify some features that may further
560 improve our understanding of the dynamics of the OVC magma reservoir.

561 Model age spectra for all four tephras are broad and contain ages that record a crystallization
562 age that is ≥ 30 kyrs older than the eruption age (Figs. 6 and 10). This finding is consistent with the
563 interpretation that the OVC zircons were most likely extracted from a crystal mush that may have
564 existed at depth long before the eruptions (Storm et al., 2011). The presence of >45 ka crystallization
565 ages in all dated MSg tephras confirms that the climactic pre-MSg Rotoiti eruption at ca. 45 ka did
566 not exhaustively depleted the OVC crystal reservoir and that a significant number of zircon crystals
567 survived this extraction event (Storm et al., 2011).

568 The model age spectrum for Unit D (Maketu) is broad and unimodal with a dominant peak at
569 ca. 62 ka. The majority of ages are older than the 45 ka caldera-forming Rotoiti eruption, documenting
570 that zircon crystallized from at least ca. 110 ka up until eruption at ca. 36 ka, and that most were
571 formed prior to the Rotoiti event (Fig. 10). In contrast to Unit D (Maketu), the model age spectra for
572 Units I (Mangaone), J (Awakeri), and K (Omataroa) are narrower and unimodal, with dominant peaks
573 at ca. 41–45 ka, documenting that these zircon grains crystallized from ca. 90 ka until their eruption
574 at ca. 30–32 ka, but that zircon crystallization peaked at ~ 41 –45 ka, shortly before, during, or shortly
575 after the Rotoiti eruption event (Fig. 10).

576 Similar patterns can be seen in the zircon U-Th age spectra reported by Charlier and Wilson
577 (2010) for Unit B (Ngamotu) and Unit I (Managone). The U-Th age spectrum for Unit B (Ngamotu)
578 (Charlier and Wilson, 2010) is similar to that obtained in this work for Unit B (Maketu), namely
579 broad, more complex, and with a major population (ca. 70 ka) older than the Rotoiti event. Notably,
580 both spectra are similar to the U-Th model age spectrum for Rotoiti zircons (Fig. 10). These data

581 suggest that Unit B (Ngamotu) and Unit D (Maketu) eruptions sampled zircon crystals from a
582 reservoir that crystallized and stored zircons long before the Rotoiti eruption. The zircon U-Th age
583 spectrum for Unit I (Mangaone) reported by Charlier and Wilson (2010) has a dominant peak at ca.
584 45 ka, coeval with the Rotoiti event, and similar to the spectra for Units I (Mangaone), J (Awakeri)
585 and K (Omataroa) from our work, suggesting that although some zircon crystals were sourced from
586 a long-lived part of the magma reservoir, the majority formed shortly before, during, or shortly after
587 the Rotoiti event. From this inference we suggest that Units I (Mangaone), J (Awakeri), and K
588 (Omataroa) eruptions tapped magma from the same domain of the reservoir and that this domain was
589 geochronologically distinct from those of Unit B (Ngamotu) and Unit D (Maketu).

590 The difference in U-Th age patterns between Old MSg and Young MSg tephras, first observed
591 by Charlier and Wilson (2010) and corroborated and complemented here, is consistent with the well-
592 documented shift in composition, temperature, and vent location within the MSg (Jurado-Chichay
593 and Walker, 2000; Smith et al., 2002, 2005). Whereas Unit B (Ngamotu) and Unit D (Maketu) tephras
594 are low-SiO₂ rhyolite and rhyodacite, respectively, erupted at 935°C presumably from the south
595 western (Unit B (Ngamotu)) and north-central (Unit D (Maketu)) parts of the OVC, Units I
596 (Mangaone), J (Awakeri), and K (Omataroa) are high-SiO₂ rhyolites that were erupted at lower
597 temperatures (755–828°C) from the eastern margin of the OVC (Jurado-Chichay and Walker, 2000;
598 Smith et al., 2002, 2005). These changes show that MSg tephras were derived from compositionally
599 and geographically distinct domains below the volcano, progressing to more evolved, cooler, and
600 possibly shallower magmas (Jurado-Chichay and Walker, 2000; Smith et al., 2002, 2005), and have
601 been attributed to ‘reorganization’ of the OVC magma reservoir following the caldera collapse at ~45
602 ka (Shane et al., 2005a; Klemetti et al., 2011; Storm et al., 2014). Based on patterns in trace element
603 and Hf isotopic data collected from Rotoiti and post-MSg tephras (Klemetti et al., 2011; Storm et al.
604 2014; Rubin et al., 2016), it has been shown that the reorganization resulted in less effective
605 interconnectedness within the OVC reservoir and its segregation into chemically distinct melt pockets
606 which did not exist prior to caldera collapse (Rubin et al., 2016). Similarly, Cole et al. (2014)

607 suggested from analyses of Unit I (Mangaone) (referred to as Kawerau Ignimbrite) that it reflected
608 two discrete magmas, hence providing evidence for the existence of multiple discrete magmas in the
609 OVC. Our geochronological results confirm the model of chemically distinct melt pockets and further
610 suggest that the degree of interconnectedness within the OVC magmatic system decreased during the
611 M₂ eruption period, most likely between the eruption of Unit D (Maketu) and Unit I (Mangaone).

612 Our new data complement the existing dataset of U-Th ages reported for other major eruptions
613 of the OVC (Charlier and Wilson, 2009; Klementi et al., 2011; Storm et al., 2011; Danišik et al.,
614 2012; Rubin et al., 2016). We acknowledge that previous studies conducted U-Th SIMS analyses on
615 different parts of zircon crystals (e.g., rim analysis on surfaces, rim analysis on sectioned and polished
616 crystal surfaces, core analysis on sectioned and polished crystal surfaces), and therefore the U-Th
617 ages may record different stages of crystal growth and not necessarily the last stage of zircon
618 crystallization. Nevertheless, the data can be used as a proxy to identify periods of zircon
619 crystallization.

620 The age spectrum of all currently available U-Th ages for the OVC (Fig. 10) confirms quasi-
621 continuous zircon crystallization under OVC since at least ca. 250 ka (Storm et al., 2011; Klemetti et
622 al., 2011). Principle component analysis using the ‘auto’ mixture model implemented in
623 DensityPlotter 7.3 (Vermeesch, 2012) revealed two dominant age populations at 49 ± 10 ka (1
624 standard deviation; 39% fraction) and 28 ± 6 ka (1 standard deviation; 28% fraction), and three
625 subordinate components at 9 ± 10 ka (1 standard deviation; 8% fraction), 79 ± 24 ka (17% fraction),
626 and 130 ± 51 ka (8% fraction). The dominant 49 ± 10 ka age population suggests that the majority of
627 zircon crystallized prior to, during, and after the caldera-forming Rotoiti eruption. This result is
628 consistent with an observed increase in the variability of zircon isotopic and trace element
629 compositions which started after ca. 60 ka and is most pronounced in post-Rotoiti zircon crystallized
630 at 20-40 ka (Storm et al., 2014; Rubin et al., 2016). It is notable that the latter age range is consistent
631 with the second dominant population of 28 ± 6 ka. It has been hypothesised that the change of

632 reservoir behaviour at ~60 ka was related to increased rate of extension and/or changes in thermal
633 flux at the OVC (Smith et al., 2005; Rubin et al., 2016).

634 635 **6. Conclusions and outlook**

636 A well-defined sequence of Mangaone Subgroup tephras from the Okataina Volcanic Centre
637 (New Zealand) was used as a natural laboratory to conduct a cross-validation experiment in which
638 we tested the accuracy of eruption ages derived using ZDD against published and new ^{14}C eruption
639 ages. ZDD eruption ages of 36.1 ± 4.4 , 31.5 ± 5.2 , 30.9 ± 5.6 , 31.2 ± 4.4 ka BP for Units D (Maketu),
640 I (Mangaone), J (Awakeri), K (Omataroa), respectively, are statistically indistinguishable from
641 optimum ^{14}C -based eruption ages on the same or stratigraphically bracketing tephras. These results
642 demonstrate the feasibility of ZDD to date eruption ages accurately.

643 The relatively low precision of our ZDD eruption ages (12–18% age uncertainties at 2σ) stems
644 primarily from the low U content in dated zircon, relatively young eruption age, and low number (i.e.,
645 7–9) of single grain replicates analysed per sample. The precision could be lowered to $<10\%$ (2σ) by
646 analysing more (~20) replicates. Although the number of replicates will always be sample specific
647 and dependent on several factors (eruption age, crystal availability, U-Th content, capacity of
648 analytical facilities, budget), in general we tentatively recommend analysing 7–20 crystals per sample
649 to achieve reasonable ZDD precision.

650 U-Th zircon crystallization data revealed that the majority of zircon crystals from Unit D
651 (Maketu) crystallized prior to the caldera-forming Rotoiti (Rotoehu) eruption at ca. 45 ka. In contrast,
652 the majority of zircon from Units I (Mangaone), J (Awakeri), and K (Omataroa) crystallized during
653 or shortly after the Rotoiti eruption and were likely derived from a distinct reservoir domain. This
654 age difference is consistent with the change in composition, temperature and vent location for Old
655 and Young MSg tephras, confirming decreasing interconnectedness within the OVC reservoir, and
656 providing further geochronological evidence for the complexity of the OVC magma reservoir.

657 Based on the new ZDD ages, and new and published ^{14}C data, we present a revised
658 geochronology for all 13 MSg tephras determined by a Bayesian age sequence model built in

ChronoModel v. 2.0 software. The revised eruption ages \pm 95% HPD regions for the MSg tephra, and Tahuna tephra, are: $42.7^{+3.7}_{-3.5}$ (Unit A), $39.6^{+4.5}_{-1.9}$ (Unit B (Ngamotu)), $38.4^{+1.7}_{-1.4}$ (Tahuna), $37.7^{+1.5}_{-1.4}$ (Unit C1 (Pupuwaharau)), $36.6^{+1.6}_{-1.0}$ (Unit C2 (Pongakawa)), $36.1^{+0.9}_{-0.8}$ (Unit D), $35.6^{+0.8}_{-1.0}$ (Unit E), $35.2^{+1.0}_{-2.0}$ (Unit F), $33.8^{+1.7}_{-2.0}$ (Unit G), $31.8^{+2.6}_{-0.8}$ (Unit H), $31.1^{+1.0}_{-0.4}$ (Unit I), $31.0^{+0.9}_{-0.8}$ (Unit J), $30.8^{+0.8}_{-1.0}$ (Unit K), $30.6^{+0.6}_{-1.5}$ ka BP (Unit L). These results refine the existing eruptive geochronology in New Zealand by constraining the beginning of the MSg phase to $42.7^{+3.7}_{-3.5}$ cal ka (Unit A), and providing comprehensive estimates of eruption ages and age uncertainties for MSg units that have not been directly dated. The frequency of eruption for the entire MSg tephra sequence of 13 episodes, emplaced over an interval of ~12,100 cal years, is every ~930 years on average.

Our study demonstrates the efficacy of ZDD to yield accurate eruption ages and highlights its potential for dating eruption events considerably younger than 1 Myr, which are challenging to date by other geochronological methods. While ZDD can be applied to numerous silicic and other zircon-producing volcanic centres on Earth, we suggest that our study may provide an impetus for wider and systematic application of ZDD in New Zealand. There is an exceptionally well-documented record of numerous regionally important, yet undated, silicic volcanic deposits aged from ca. 50 ka to 1 Ma in New Zealand, many of which would be excellent targets for development of a high-precision tephrostratigraphic framework spanning well beyond the conventional limits of ^{14}C .

Acknowledgements

MD was supported by the AuScope NCRIS2 program, Australian Research Council (ARC) Discovery funding scheme (DP160102427) and Curtin Research Fellowship. Part of this research was undertaken using the SEM instrumentation (ARC LE0775553) at the John de Laeter Centre, Curtin University. We acknowledge the help of A.S. Kumara, A. Frew, B. Ware and E. Miller with mineral separation, zircon dissolution, solution ICP-MS analyses and SEM imaging, and K. Holt for generating an early version of Table 2. MD thanks I. Dunkl for sharing PepiFLEX software for ICP-MS data reduction and P. Lanos for providing guidance on Bayesian modelling in ChronoModel. DJL acknowledges the New Zealand Marsden

685 Fund *Te Pūta Rangahau a Marsden* for supporting tephra-paleosol research in the Bay of Plenty area
686 for the project “New Views from old soils: testing the reconstruction of environmental and climatic
687 change using genetic signals preserved in buried paleosols” (10-UOW-056). The paper is an output
688 of the Commission on Tephrochronology (COT) of the International Association of Volcanism and
689 Chemistry of the Earth’s Interior (IAVCEI).

690

691 **Table captions**

692

693 **Table 1:** Summary of stratigraphy, nomenclature, and volumes for MSg tephras.

694 **Table 2:** Summary of ¹⁴C data.

695 **Table 3:** ZDD data summary.

696

697 **Supplementary Table S1:** ChronoModel input data.

698 **Supplementary Table S2:** U-Th data.

699 **Supplementary Table S3:** ZDD data.

700 **Supplementary Table S4:** ¹⁴C data.

701 **Supplementary Table S5:** Summary of Bayesian age sequence modelling results.

702

703 **Figure captions**

704

705 **Figure 1:** Secondary electron images of two zircon crystals (top panels – planar view; bottom panels
706 – perspective view) after SIMS analysis showing the minimal material consumption of CAMECA
707 ims 1280-HR required for U-Th analysis. Sputtered elliptical craters are 40 × 25 µm in area and 4 µm
708 deep, and so the majority of the crystal remains intact for subsequent (U-Th)/He analysis.

709

710 **Figure 2:** Distribution of the most widespread MSg tephras in the North Island of New Zealand
711 (modified after Jurado-Chichay and Walker, 2000). OVC – Okataina Volcanic Centre; TVZ – Taupo
712 Volcanic Zone, simplified boundary after Wilson et al. (2009). *Inset:* Location map, New Zealand.

713

714 **Figure 3:** Summary of published ^{14}C , new ^{14}C , and new ZDD ages for MSg tephras (and Tahuna
715 tephra which did not originate in OVC) arranged in stratigraphic order. The ages are displayed as 1σ
716 (bars) and 2σ (whiskers) age ranges. Conventional ^{14}C ages were calibrated to calendar years (cal
717 years BP) in OxCal 4.3 software (Bronk Ramsey, 2009) using the SHCal13 calibration curve (Hogg
718 et al., 2013). Data compiled from Vucetich and Pullar (1969), Pullar and Heine (1971), Nairn (1981),
719 McGlone et al. (1984), Froggatt and Lowe (1990), Jurado-Chichay and Walker (2000), Shane et al.
720 (2006), Molloy et al. (2009), Loame et al. (2019), and our study.

721

722 **Figure 4:** Images showing the stratigraphy of MSg deposits and the positions of the materials we
723 sampled at two locations for ZDD and ^{14}C dating. A – Unit I (Mangaone) tephra section in Bowditch
724 Quarry was sampled for zircon (NZ18-3) and charcoal (BDQ-1). Uppermost unit (ash and pumice
725 lapilli) was deposited by a pyroclastic flow (density current) (Howorth, 1975). B – Close-up of the
726 BDQ-1 charcoal material. C – Section showing Unit J (Awakeri) and Unit K (Omataroa) tephras in
727 Bowditch Quarry. D – Section at Little Waihi Road sampled for Unit D (Maketu) and Unit F
728 (Hauparu) tephras (the latter did not yield zircon of required quality). Note that Rotoehu Ash
729 represents tephra-fall beds associated with the eruption of the Rotoiti Tephra Formation (Froggatt and
730 Lowe, 1990). Spade for scale is ca. 120 cm long.

731

732 **Figure 5:** ^{238}U - ^{230}Th isochron diagram for MSg tephras dated in this study showing that all zircon
733 isotopic ratios are in secular disequilibrium (i.e., all ellipses plot to the right of the equiline).
734 Confidence ellipses are plotted at 95% level of confidence. The diagram was constructed in IsoplotR

735 (Vermeesch, 2018); isochrons (dashed grey lines) are based on mean Th/U whole rock composition
736 of 0.639 (blue diamond).

737

738 **Figure 6:** Zircon U-Th and (U-Th)/He ages (blue squares and red diamonds, respectively) with 1σ
739 analytical uncertainties for MSg tephras analysed by ZDD displayed in ranked order plots. Kernel
740 density estimation (KDE) and probability distribution function (PDF) curves (dotted and dashed
741 green curves, respectively) for U-Th data were constructed in DensityPlotter (Vermeesch, 2012).
742 Vertical dashed orange lines and yellow rectangles indicate the ZDD eruption ages and their 95%
743 confidence intervals, respectively, calculated as error weighted means in Isoplot (Ludwig, 2012). The
744 samples are arranged in stratigraphic order to allow easy comparison of ZDD eruption ages. MSWD
745 – mean square of weighted deviation. The full dataset can be found in Table 3 and Supplementary
746 Tables S2 and S3.

747

748 **Figure 7:** *Left:* Histograms showing posterior distributions of mean values for (U-Th)/He ages that
749 represent the Bayesian estimates of most probable eruption ages and their uncertainties (horizontal
750 bars represent 95% high density intervals, HDI). *Right:* Histograms showing posterior differences of
751 the mean (U-Th)/He values predicted by Bayesian analysis for stratigraphically adjacent tephras. The
752 differences of the mean values serve as a test to decide whether there is a credible difference between
753 the eruption ages of the dated tephras. For Units I (Mangaone), J (Awakeri), and K (Omataroa), the
754 95% HDI of the difference of means are quasi-symmetrically distributed around zero, and there is no
755 statistically credible difference in their eruption ages. For Units D (Maketu) and I (Mangaone)
756 (bottom right diagram), in contrast, the 95% HDI marginally overlaps with zero and >90% of the
757 predicted values are >0, and therefore we can conclude that there is >90% probability that the eruption
758 ages of these two tephras are credibly different.

759

760 **Figure 8:** Comparison of Bayesian age sequence modelling results based on different input
761 parameters as specified in the text. Note the insignificant difference in ages (solid lines) and 95%
762 HPD regions between the three tested models (see text), demonstrating the robustness of the adopted
763 Bayesian approach and its immunity to anomalous ages. Numerical results can be found in
764 Supplementary Table S4.

766 **Figure 9:** Posterior distribution graphs for probability densities (curves) of the eruption ages
767 predicted by Bayesian age sequence model in ChronoModel v. 2.0. The 95% highest posterior density
768 (HDP) regions are represented by the horizontal bars above the curves and by the grey filled areas
769 under the curves. *Labels:* name of the eruption/tephra; the mode of the posterior distribution (i.e.,
770 maximum a posterior probability or ‘MAP’) in cal ka BP; 95% HPD in cal ka BP. Numerical results
771 can be found in Supplementary Table S4.

773 **Figure 10:** Compilation of available U-Th zircon crystallization ages for Rotoiti and post-
774 Rotoiti eruptions from the OVC. Kernel density estimates (KDE; dashed lines) and probability
775 density fFunction (PDF, solid lines) curves were constructed in Density Plotter v.7.3
776 (Vermeesch, 2012); data-points represented by grey tick marks; eruption ages represented by
777 vertical red bars. Major components identified using Density Plotter v.7.3 are shown in the
778 top panel; identified age populations (P1–5) are represented by Gaussian curves as well as
779 described by age \pm standard deviation (in ka) and fraction (in %); non-consolidated volumes in
780 km³ (brown numbers) after Jurado-Chichay and Walker (2000) and Wilson et al. (2009). The age
781 for the caldera-forming Rotoiti eruption is projected across all the post-Rotoiti eruptions. Note that
782 Unit I (Mangaone) eruption was the first one to provide the majority of zircon crystals that formed
783 during or after the Rotoiti eruption, whereas Unit B (Ngamotu) and Unit D (Maketu) sourced
784 mostly pre-Rotoiti zircon crystals. Also note that the majority of zircon crystals erupted from
785 OVC in the past 45 kyrs formed shortly before, during, and shortly after the Rotoiti event as
suggested by the major age population of 49 ± 10 ka comprising 39% of all dated crystals. This
finding is consistent with the onset of increasing diversification of trace element and

786 isotopic compositions in OVC zircon starting at ca. 60 ka (Rubin et al., 2016) and major
787 ‘reorganization’ of the OVC caldera during and after the Rotoiti event (Shane et al., 2005a; Smith et
788 al., 2005; Storm et al., 2014; Rubin et al., 2016).

789

790 **Supplementary Figure S1:** Schematic structure of the Bayesian age model constructed in
791 ChronoModel v.2 software. Blue arrows indicate stratigraphic relationships in the sequence. Input
792 parameters: ^{14}C and ZDD ages with 1 sigma uncertainties; for tephras with no directly measured
793 eruption ages the eruption interval was defined as typo-chronological age range spanning from age
794 of underlying unit $+2\sigma$ uncertainty to age of overlying unit -2σ uncertainty.

795 **References**

796

797 Berryman, K.R., 1992: A stratigraphic age of Rotoehu Ash and late Pleistocene climate

798 interpretation based on marine terrace chronology, Mahia Peninsula, North Island, New

799 Zealand. New Zealand Journal of Geology and Geophysics, 35, 1-7.

800 Blondes, M. S., Reiners, P. W., Edwards, B. R., Biscontin, A., 2007: Dating young basalt eruptions

801 by (U-Th)/He on xenolithic zircons. Geology, 35(1), 17-20.

802 Boehnke, P., Watson, E. B., Trail, D., Harrison, T. M., Schmitt, A. K., 2013: Zircon saturation re-

803 revisited. Chemical Geology, 351, 324-334.

804 Briggs, R. M., Lowe, D. J., Esler, W. R., Smith, R. T., Henry, M. A. C., Wehrmann, H., Manning, D.

805 A., 2006: Geology of the Maketu area, Bay of Plenty, North Island, New Zealand - Sheet

806 V14 1:50 000. Department of Earth Sciences, University of Waikato, Occasional Report 26,

807 44 pp.

808 Bronk Ramsey, C., 2009: Bayesian analysis of radiocarbon dates. Radiocarbon 51, 337-360.

809 Burgess, S. D., Coble, M. A., Vazquez, J. A., Coombs, M. L., Wallace, K. L., 2019: On the eruption

810 age and provenance of the Old Crow tephra. Quaternary Science Reviews, 207, 64-79.

811 Charlier, B. L. A., Wilson, C. J. N., 2010: Chronology and evolution of caldera-forming and post-

812 caldera magma systems at Okataina Volcano, New Zealand from zircon U–Th model-age

813 spectra. Journal of Petrology, 51(5), 1121-1141.

814 Charlier, B. L., Peate, D. W., Wilson, C. J., Lowenstern, J. B., Storey, M., Brown, S. J., 2003:

815 Crystallisation ages in coeval silicic magma bodies: ^{238}U – ^{230}Th disequilibrium evidence

816 from the Rotoiti and Earthquake Flat eruption deposits, Taupo Volcanic Zone, New Zealand.

817 Earth and Planetary Science Letters, 206(3-4), 441-457.

818 Cherniak, D. J., Watson, E. B., 2001: Pb diffusion in zircon. Chemical Geology, 172(1), 5-24.

819 Chesner, C. A., Barbee, O. A., McIntosh, W. C., 2020: The enigmatic origin and emplacement of the
820 Samosir Island lava domes, Toba Caldera, Sumatra, Indonesia. *Bulletin of Volcanology*,
821 82(3), 1-20.

822 Coble, M. A., Burgess, S. D., Klemetti, E. W., 2017: New zircon (U-Th)/He and U/Pb eruption age
823 for the Rockland tephra, western USA. *Quaternary Science Reviews*, 172, 109-117.

824 Cole, J.W., Spinks, K.D., Deering, C.D., Nairn, I.A., Leonard, G.S., 2010: Volcanic and structural
825 evolution of the Okataina Volcanic Centre; dominantly silicic volcanism associated with the
826 Taupo Rift, New Zealand. *Journal of Volcanology and Geothermal Research*, 190, 123–
827 135.

828 Cole, J.W., Deering, C.D., Nairn, Burt, R.M., Sewell, S., Shane, P.A.R., Matthews, N.E., 2014:
829 Okataina Volcanic Centre, Taupo Volcanic Zone, New Zealand: A review of volcanism and
830 synchronous pluton development in an active, dominantly silicic caldera system. *Earth-*
831 *science Reviews*, 128, 1-17.

832 Danišík, M., McInnes, B. I., Kirkland, C. L., McDonald, B. J., Evans, N. J., Becker, T., 2017b: Seeing
833 is believing: Visualization of He distribution in zircon and implications for thermal history
834 reconstruction on single crystals. *Science Advances*, 3(2), e1601121.

835 Danišík, M., Schmitt, A. K., Stockli, D. F., Lovera, O. M., Dunkl, I., & Evans, N. J., 2017a:
836 Application of combined U-Th-disequilibrium/U-Pb and (U-Th)/He zircon dating to
837 tephrochronology. *Quaternary Geochronology*, 40, 23-32.

838 Danišík, M., Shane, P., Schmitt, A. K., Hogg, A., Santos, G. M., Storm, S., Evans, N. J., Fifield, L.
839 K., Lindsay, J. M., 2012: Re-anchoring the late Pleistocene tephrochronology of New
840 Zealand based on concordant radiocarbon ages and combined $^{238}\text{U}/^{230}\text{Th}$ disequilibrium and
841 (U-Th)/He zircon ages. *Earth and Planetary Science Letters*, 349-350, 240-250.

842 Evans, N. J., Byrne, J. P., Keegan, J. T., Dotter, L. E., 2005: Determination of uranium and thorium
843 in zircon, apatite, and fluorite: application to laser (U-Th)/He thermochronology. *Journal of*
844 *Analytical Chemistry*, 60(12), 1159-1165.

845 Farley, K.A., Kohn, B.P., Pillans, B., 2002: The effects of secular disequilibrium on (U–Th)/He
846 systematics and dating of Quaternary volcanic zircon and apatite. *Earth and Planetary*
847 *Science Letters*, 201, 117-125.

848 Farley, K.A., Wolf, R.A., Silver, L.T., 1996: The effects of long alpha-stopping distances on (U-
849 Th)/He ages. *Geochimica et Cosmochimica Acta*, 60, 4223-4229.

850 Flude, S., Storey, M., 2016: $^{40}\text{Ar}/^{39}\text{Ar}$ age of the Rotoiti Breccia and Rotoehu Ash, Okataina Volcanic
851 Complex, New Zealand, and identification of heterogeneously distributed excess ^{40}Ar in
852 supercooled crystals. *Quaternary Geochronology*, 33, 13-23.

853 Friedrichs, B., Schmitt, A. K., McGee, L., Turner, S., 2020: U-Th whole rock data and high spatial
854 resolution U-Th disequilibrium and U-Pb zircon ages of Mt. Erciyes and Mt. Hasan
855 Quaternary stratovolcanic complexes (Central Anatolia). *Data in Brief*, 105113.

856 Froggatt, P. C., Lowe, D. J., 1990: A review of late Quaternary silicic and some other tephra
857 formations from New Zealand: their stratigraphy, nomenclature, distribution, volume and
858 age. *New Zealand Journal of Geology and Geophysics* 33, 89-109.

859 Gençlioğlu-Kuşcu, G., Uslular, G., Danišik, M., Koppers, A., Miggins, D. P., Friedrichs, B., &
860 Schmitt, A. K., 2020: U–Th disequilibrium, (U–Th)/He and $^{40}\text{Ar}/^{39}\text{Ar}$ geochronology of
861 distal Nisyros Kyra tephra deposits on Datça peninsula (SW Anatolia). *Quaternary*
862 *Geochronology*, 55, 101033, 1-13.

863 Grant-Taylor, T. L., Rafter, T. A., 1971: New Zealand radiocarbon age measurements — 6. New
864 Zealand Journal of Geology and Geophysics, 14, 364-402.

865 Harangi, S., Lukács, R., Schmitt, A.K., Dunkl, I., Molnár, K., Kiss, B., Seghedi, I., Novothny, Á.,
866 Molnár, M., 2015: Constraints on the timing of Quaternary volcanism and duration of
867 magma residence at Ciomadul volcano, east-central Europe, from combined U-Th/He and
868 U-Th zircon geochronology. *Journal of Volcanology and Geothermal Research*, 301, 66-80.

869 Hodder, A.P.W., Green, B.E., Lowe, D.J., 1990: A two-stage model for the formation of clay minerals
870 from tephra derived volcanic glass. *Clay Minerals*, 25, 313-327.

871 Hogg, A.G., McCraw, J.D., 1983: Late Quaternary tephras of Coromandel Peninsula, North Island,
872 New Zealand: a mixed peralkaline and calcalkaline tephra sequence. *New Zealand Journal*
873 *of Geology and Geophysics*, 26, 163-187.

874 Hogg, A. G., Fifield, L. K., Palmer, J. G., Turney, C. S., Galbraith, R., 2007: Robust radiocarbon
875 dating of wood samples by high-sensitivity liquid scintillation spectroscopy in the 50–70 kyr
876 age range. *Radiocarbon*, 49(2), 379-391.

877 Hogg, A. G., Hua, Q., Blackwell, P. G., Niu, M., Buck, C. E., Guilderson, T. P., Heaton, T.J., Palmer,
878 J.G., Reimer, P.J., Reimer, R.W., Turney, C.S.M., Zimmerman, S.R.H., 2013: SHCal13
879 Southern Hemisphere calibration, 0–50,000 years cal BP. *Radiocarbon*, 55(4), 1889-1903.

880 Hogg, A.G., Wilson, C.J.N., Lowe, D.J., Turney, C.S.M., White, P., Lorrey, A.M., Manning, S.W.,
881 Palmer, J.G., Bury, S., Brown, J., Southon, J., Petchey, F., 2019. Wiggle-match radiocarbon
882 dating of the Taupo eruption. *Nature Communications*, 10, 4669.

883 Hopkins, J. L., Wilson, C. J., Millet, M. A., Leonard, G. S., Timm, C., McGee, L. E., Smith, I. E. M.,
884 Smith, E. G., 2017: Multi-criteria correlation of tephra deposits to source centres applied in
885 the Auckland Volcanic Field, New Zealand. *Bulletin of Volcanology*, 79(7), 55,
886 <https://doi.org/10.1007/s00445-017-1131-y>

887 Hourigan, J. K., Reiners, P. W., Brandon, M. T., 2005: U-Th zonation dependent alpha-ejection in
888 (U-Th)/He chronometry, Part I: Theory. *Geochimica et Cosmochimica Acta*, 69, 3349-3365.

889 Houghton, B.F., Weaver, S.D., Wilson, C.J.N., Lanphere, M.A., 1992. Evolution of a Quaternary
890 peralkaline volcano: Mayor Island, New Zealand. *Journal of Volcanology and Geothermal*
891 *Research*, 51, 217-236.

892 Howorth, R., 1975: New formations of late Pleistocene tephras from the Okataina Volcanic Centre,
893 New Zealand. *New Zealand Journal of Geology and Geophysics*, 18(5), 683-712.

894 Howorth, R., 1981: Editorial. In: Howorth, R. et al. (eds). *Proceedings of tephra workshop*. *Geology*
895 *Department Victoria University of Wellington Publication*, 20, 1-4.

896 Ito, H., Danišík, M., 2020: Dating late Quaternary events by the combined U- Pb LA- ICP- MS and
897 (U- Th)/He dating of zircon: a case study on Omachi Tephra suite (central Japan). *Terra*
898 *Nova*, 32(2), 134-140.

899 Jurado-Chichay, Z., Walker, G. P. L., 2000: Stratigraphy and dispersal of the Mangaone Subgroup
900 pyroclastic deposits, Okataina Volcanic Centre, New Zealand. *Journal of Volcanology and*
901 *Geothermal Research*, 104(1-4), 319-380.

902 Jurado-Chichay, Z., Walker, G. P. L., 2001a: The intensity and magnitude of the Mangaone subgroup
903 plinian eruptions from Okataina Volcanic Centre, New Zealand. *Journal of Volcanology and*
904 *Geothermal Research*, 111, 219-237.

905 Jurado-Chichay, Z., Walker, G. P. L., 2001b: Variability of plinian fall deposits: examples from
906 Okataina Volcanic Centre, New Zealand. *Journal of Volcanology and Geothermal Research*,
907 111, 239-263.

908 Kirkland, C. L., Danišík, M., Marsden, R., Piilonen, P., Barham, M., Sutherland, L., 2020: Dating
909 young zircon: a case study from Southeast Asian megacrysts. *Geochimica et Cosmochimica*
910 *Acta*, 274, 1-19.

911 Klemetti, E. W., Deering, C. D., Cooper, K. M., Roeske, S. M., 2011: Magmatic perturbations in the
912 Okataina Volcanic Complex, New Zealand at thousand-year timescales recorded in single
913 zircon crystals. *Earth and Planetary Science Letters*, 305(1-2), 185-194.

914 Lanos, P., Philippe, A., 2017: Hierarchical Bayesian modeling for combining dates in archaeological
915 context. *Journal de la Société Française de Statistique*, 158, 72-88.

916 Lanos, P., Dufresne, P., 2019: ChronoModel version 2.0: User manual. Available from:
917 <http://www.chronomodel.com>

918 Lanos, P., Philippe, A., 2018: Event date model: a robust Bayesian tool for chronology building.
919 *Communications for Statistical Applications and Methods*, Korean Statistical Society (KSS)
920 /Korean International Statistical Society (KISS), 25 (2), 131-157.

921 Leonard, G.S., Begg, J.G., Wilson, C.J.J. (compilers) 2010: Geology of the Rotorua area: scale 1:
 922 250,000. Institute of Geological and Nuclear Sciences 1: 250,000 geological map 5. 1 sheet
 923 and 99 pp. Institute of Geological and Nuclear Sciences, Lower Hutt.

924 Lian, O. B., Shane, P. A., 2000: Optical dating of paleosols bracketing the widespread Rotoehu
 925 tephra, North Island, New Zealand. *Quaternary Science Reviews*, 19(16), 1649-1662.

926 Loame, R. C., Villamor, P., Lowe, D. J., Milicich, S. D., Pittari, A., Barker, S. L., Rae, A., Gómez-
 927 Vasconcelos, M. G., Martinez-Martos, M., Ries, W. F., 2019: Using paleoseismology and
 928 tephrochronology to reconstruct fault rupturing and hydrothermal activity since c. 40 ka in
 929 Taupo Rift, New Zealand. *Quaternary International*, 500, 52-70.

930 Lowe, D.J., Percival, H.J., 1993: Clay mineralogy of tephra and associated paleosols and soils, and
 931 hydrothermal deposits, North Island. Guide book for New Zealand Pre-Conference Field
 932 Trip Fl, 10th International Clay Conference, Adelaide, Australia. 110 p.

933 Lowe, D.J., Hogg, A.G., 1995: Age of the Rotoehu Ash. *New Zealand Journal of Geology and*
 934 *Geophysics*, 38, 399-402.

935 Ludwig, K. R., 2012: User's Manual for Isoplot 3.75: A geochronological toolkit for Microsoft Excel.
 936 Berkeley Geochronology Center Special Publication, 5, 75.

937 Mark, D. F., Renne, P. R., Dymock, R. C., Smith, V. C., Simon, J. I., Morgan, L. E., Staff, R. A.,
 938 Ellis, B. S., Pearce, N. J., 2017: High-precision $^{40}\text{Ar}/^{39}\text{Ar}$ dating of Pleistocene tuffs and
 939 temporal anchoring of the Matuyama-Brunhes boundary. *Quaternary Geochronology*, 39, 1-
 940 23.

941 McGlone, M. S., Howorth, R., Pullar, W. A., 1984: Late Pleistocene stratigraphy, vegetation and
 942 climate of the Bay of Plenty and Gisborne regions, New Zealand. *New Zealand Journal of*
 943 *Geology and Geophysics*, 27, 327-350.

944 Molloy, C., Shane, P., Augustinus, P., 2009: Eruption recurrence rates in a basaltic volcanic field
 945 based on tephra layers in maar sediments: implications for hazards in the Auckland volcanic
 946 field. *Geological Society of America Bulletin*, 121(11-12), 1666-1677.

947 Molnár, K., Harangi, S., Lukács, R., Dunkl, I., Schmitt, A. K., Kiss, B., Garamhegyi, T., Seghedi, I.,
 948 2018: The onset of the volcanism in the Ciomadul Volcanic Dome Complex (eastern
 949 Carpathians): eruption chronology and magma type variation. *Journal of Volcanology and*
 950 *Geothermal Research*, 354, 39-56.

951 Mucek, A. E., Danišík, M., de Silva, S. L., Miggins, D. P., Schmitt, A. K., Pratomo, I., Koppers, A.,
 952 Gillespie, J., (in review): Bayesian analysis of coupled $^{40}\text{Ar}/^{39}\text{Ar}$ and (U-Th)/He
 953 thermochronometry reveals cold-stored regions of long-lived warm magma erupted at Toba
 954 Caldera, Sumatra. Re-submitted to *Geology* in April 2020.

955 Mucek, A. E., Danišík, M., de Silva, S. L., Schmitt, A. K., Pratomo, I., and Coble, M. A., 2017: Post-
 956 supereruption recovery at Toba Caldera. *Nature Communications*, 8(1), 1-9.

957 Nairn, I.A. 1972: Rotoehu Ash and Rotoiti Breccia Formation, Taupo Volcanic Zone, New Zealand.
 958 *New Zealand Journal of Geology and Geophysics*, 15, 251-261.

959 Nairn, I., 1981: Some studies of the geology, volcanic history, and geothermal resources of the
 960 Okataina Volcanic Centre, Taupo Volcanic Zone, New Zealand. Unpublished Ph.D. thesis,
 961 lodged in the Library, Victoria University of Wellington, Wellington.

962 Nairn, I.A., 1989: Sheet V16AC Tarawera – Geological Map of New Zealand 1:50 000. New Zealand
 963 Department of Scientific and Industrial Research, Wellington.

964 Nairn, I.A., 2002: Geology of the Okataina Volcanic Centre, scale 1: 50000. Institute of Geological
 965 and Nuclear Sciences, Lower Hutt, New Zealand.

966 Newnham, R.M., Lowe, D.J., Green, J.D., Turner, G.M., Harper, M.A., McGlone, M.S., Stout, S.L.,
 967 Horie, S., Froggatt, P.C., 2004: A discontinuous ca. 80 ka record of Late Quaternary
 968 environmental change from Lake Omapere, Northland, New Zealand. *Palaeogeography,*
 969 *Palaeoclimatology, Palaeoecology*, 207, 165-198.

970 Nilsson, A., Muscheler, R., Snowball, I., Aldahan, A., Possnert, G., Augustinus, P., Atkin, D.,
 971 Stephens, T., 2011: Multi-proxy identification of the Laschamp geomagnetic field excursion

972 in Lake Pupuke, New Zealand. *Earth and Planetary Science Letters*, 311, 155-164.
 973 <http://dx.doi.org/10.1016/j.epsl.2011.08.050>.

974 Paces, J.B., Miller, J. D. Jr., 1993: Precise U-Pb ages of Duluth Complex and related mafic intrusions,
 975 northeastern Minnesota: geochronological insights to physical, petrogenetic, paleomagnetic,
 976 and tectonomagnetic processes associated with the 1.1 Ga Midcontinent Rift system. *Journal*
 977 *of Geophysical Research*, 98(B8), 13997-14013.

978 Peti, L., Augustinus, P.C. 2019: Stratigraphy and sedimentology of the Orakei maar lake sediment
 979 sequence (Auckland Volcanic Field, New Zealand). *Scientific Drilling*, 25, 47-56.

980 Pillans, B., Wright, I., 1992: Late Quaternary tephrostratigraphy from the southern Havre Trough-
 981 Bay of Plenty, northeast New Zealand. *New Zealand Journal of Geology and Geophysics*,
 982 35(2), 129-143.

983 Pullar, W. A., Heine, J. C., 1971: Ages, inferred from ^{14}C dates, of some tephra and other deposits
 984 from Rotorua, Taupo, Bay of Plenty, Gisborne, and Hawke's Bay districts. *Proceedings,*
 985 *Radiocarbon Users' Conference*, 17-18 August 1971, Lower Hutt, New Zealand, pp. 117-
 986 138.

987 Pullar, W. A., Birrell, K. S., Heine, J. C., 1973: Named tephras and tephra formations occurring in
 988 the central North Island, with notes on derived soils and buried paleosols. *New Zealand*
 989 *Journal of Geology and Geophysics*, 16 (3), 497-518.

990 Reiners, P. W., Spell, T. L., Nicolescu, S., Zanetti, K. A., 2004. Zircon (U-Th)/He
 991 thermochronometry: He diffusion and comparisons with $^{40}\text{Ar}/^{39}\text{Ar}$ dating. *Geochimica et*
 992 *Cosmochimica Acta*, 68, 1857-1887.

993 Reiners, P.W., 2005: Zircon (U-Th)/He Thermochronometry, in Reiners, P.W. and Ehlers, T.A.
 994 (Eds.), *Thermochronology, Reviews in Mineralogy and Geochemistry*, v. 58, p. 151-176.

995 Rosman, K. J. R., Taylor, P. D. P., 1998: Isotopic compositions of the elements 1997 (Technical
 996 Report). *Pure and Applied Chemistry*, 70(1), 217-235.

997 Rubin, A. E., Cooper, K. M., Leever, M., Wimpenny, J., Deering, C., Rooney, T., Gravley, D., Yin,
 998 Q-Z., 2016: Changes in magma storage conditions following caldera collapse at Okataina
 999 Volcanic Center, New Zealand. *Contributions to Mineralogy and Petrology*, 171, 1-18.

1000 Sakata, S., Hirakawa, S., Iwano, H., Danhara, T., Guillong, M., Hirata, T., 2017: A new approach for
 1001 constraining the magnitude of initial disequilibrium in Quaternary zircons by coupled
 1002 uranium and thorium decay series dating. *Quaternary Geochronology*, 38, 1-12. <https://doi.org/10.1016/j.quageo.2016.11.002>
 1003

1004 Santos, G. M., Bird, M. I., Pillans, B., Fifield, L. K., Alloway, B. V., Chappell, J., Hausladen, P. A.,
 1005 Arneeth, A., 2001: Radiocarbon dating of wood using different pretreatment procedures:
 1006 application to the chronology of Rotoehu Ash, New Zealand. *Radiocarbon*, 43(2A), 239-
 1007 248.

1008 Schmitt, A.K., Stockli, D.F., Lindsay, J.M., Robertson, R., Lovera, O.M., Kislitsyn, R., 2010a.
 1009 Episodic growth and homogenization of plutonic rocks in arc volcanoes from combined U-
 1010 Th and (U-Th)/He zircon dating. *Earth and Planetary Science Letters*, 295, 91-103.

1011 Schmitt, A.K., Stockli, D.F., Niedermann, S., Lovera, O.M., Hausback, B.P., 2010b: Eruption ages
 1012 of Las Tres Vírgenes volcano (Baja California): a tale of two helium isotopes. *Quaternary*
 1013 *Geochronology*, 5, 503-511.

1014 Schmitt, A. K., 2007: Letter: Ion microprobe analysis of $(^{231}\text{Pa})/(^{235}\text{U})$ and an appraisal of
 1015 protactinium partitioning in igneous zircon. *American Mineralogist*, 92(4), 691-694.

1016 Schmitt, A. K., 2011: Uranium series accessory crystal dating of magmatic processes. *Annual*
 1017 *Reviews in Earth and Planetary Sciences*, 39, doi:10.1146/annurev-earth-040610-133330.

1018 Schmitt, A. K., Danišik, M., Evans, N., Siebel, W., Kiemele, E., Aydin, F., Harvey, J. C., 2011:
 1019 Acigöl rhyolite field, Central Anatolia (part 1): high-resolution dating of eruption episodes
 1020 and zircon growth rates. *Contributions to Mineralogy and Petrology*, 162(6), 1233-1247.

1021 Schmitt, A. K., Klitzke, M., Gerdes, A., Schäfer, C., 2017: Zircon hafnium–oxygen isotope and trace
 1022 element petrochronology of intraplate volcanic rocks from the Eifel (Germany) and

1023 implications for mantle versus crustal origins of zircon megacrysts. *Journal of Petrology*,
 1024 58(9), 1841-1870.

1025 Schmitt, A. K., Martín, A., Stockli, D. F., Farley, K. A., Lovera, O. M., 2012: (U-Th)/He zircon and
 1026 archaeological ages for a late prehistoric eruption in the Salton Trough (California, USA).
 1027 *Geology*, 41(1), 7-10.

1028 Schmitt, A. K., Stockli, D. F., Hausback, B. P., 2006. Eruption and magma crystallization ages of Las
 1029 Tres Vírgenes (Baja California) constrained by combined $^{230}\text{Th}/^{238}\text{U}$ and (U-Th)/He dating
 1030 of zircon. *Journal of Volcanology and Geothermal Research*, 158, 281-295.

1031 Shane, P., Sandiford, A., 2003: Paleovegetation of marine isotope stages 4 and 3 in Northern New
 1032 Zealand and the age of the widespread Rotoehu tephra. *Quaternary Research*, 59(3), 420-
 1033 429.

1034 Shane, P., Nairn, I. A., Smith, V. C., 2005a: Magma mingling in the ~50 ka Rotoiti eruption from
 1035 Okataina Volcanic Centre: implications for geochemical diversity and chronology of large
 1036 volume rhyolites. *Journal of Volcanology and Geothermal Research*, 139, 295-313.

1037 Shane, P.A.R., Smith, V.C., Nairn, I.A., 2005b. High temperature rhyodacites of the 36 ka Hauparu
 1038 pyroclastic eruption, Okataina Volcanic Centre, New Zealand: change in a silicic magmatic
 1039 system following caldera collapse. *J. Volcanol. Geotherm. Res.*, 147, pp.357-376.

1040 Shane, P., Sikes, E.L., Guilderson, T.P., 2006: Tephra beds in deep-sea cores off northern New
 1041 Zealand: implications for the history of Taupo Volcanic Zone, Mayor Island and White
 1042 Island volcanoes. *Journal of Volcanology and Geothermal Research*, 154, 276-290.

1043 Siddall, M., Rohling, E.J., Thompson, W.G., Waelbroeck, C., 2008. Marine isotope stage 3 sea level
 1044 fluctuations: data synthesis and new outlook. *Reviews of Geophysics*, 46, RG4003.

1045 Sisson, T. W., Schmitt, A. K., Danišík, M., Calvert, A. T., Pempena, N., Huang, C. Y., Shen, C. C.,
 1046 2019: Age of the dacite of Sunset Amphitheater, a voluminous Pleistocene tephra from
 1047 Mount Rainier (USA), and implications for Cascade glacial stratigraphy. *Journal of*
 1048 *Volcanology and Geothermal Research*, 376, 27-43.

1049 Smith, V., Shane, P., 2002: Geochemical characteristics of the widespread Tahuna Tephra. New
1050 Zealand Journal of Geology and Geophysics, 45, 103-107.

1051 Smith, V. C., Shane, P., Smith, I. E. M., 2002: Tephrostratigraphy and geochemical fingerprinting of
1052 the Mangaone Subgroup tephra beds, Okataina Volcanic Centre, New Zealand. New Zealand
1053 Journal of Geology and Geophysics, 45(2), 207-219.

1054 Smith, V. C., Shane, P., Nairn, I. A., 2005: Trends in rhyolite geochemistry, mineralogy, and magma
1055 storage during the last 50 kyr at Okataina and Taupo volcanic centres, Taupo Volcanic Zone,
1056 New Zealand. Journal of Volcanology and Geothermal Research, 148(3-4), 372-406.

1057 Spencer, C. J., Kirkland, C. L., Taylor, R. J., 2016: Strategies towards statistically robust
1058 interpretations of in situ U–Pb zircon geochronology. Geoscience Frontiers, 7(4), 581-589.

1059 Storm, S., Schmitt, A. K., Shane, P., Lindsay, J. M., 2014: Zircon trace element chemistry at sub-
1060 micrometer resolution for Tarawera volcano, New Zealand, and implications for rhyolite
1061 magma evolution. Contributions to Mineralogy and Petrology, 167(4), 1000.

1062 Storm, S., Shane, P., Schmitt, A. K., Lindsay, J. M., 2011: Contrasting punctuated zircon growth in
1063 two syn-erupted rhyolite magmas from Tarawera volcano: insights to crystal diversity in
1064 magmatic systems. Earth and Planetary Science Letters, 301(3-4), 511-520.

1065 Storm, S., Shane, P., Schmitt, A. K., Lindsay, J. M., 2012: Decoupled crystallization and eruption
1066 histories of the rhyolite magmatic system at Tarawera volcano revealed by zircon ages and
1067 growth rates. Contributions to Mineralogy and Petrology, 163(3), 505-519.

1068 Thompson, B.N., 1968. Age of Rotoiti Breccia. New Zealand Journal of Geology and Geophysics,
1069 11(5), 1189-1191.

1070 Ulusoy, İ., Sarıkaya, M. A., Schmitt, A. K., Şen, E., Danišík, M., Gümüş, E., 2019: Volcanic eruption
1071 eye-witnessed and recorded by prehistoric humans. Quaternary Science Reviews, 212, 187-
1072 198.

1073 Vandergoes, M. J., Hogg, A. G., Lowe, D. J., Newnham, R. M., Denton, G. H., Southon, J., Barrell,
1074 D.J.A., Wilson, C.J.N., McGlone, M.S., Allan, A.S.R., Almond, P.C., Petchey, F., Dabell,

1075 K., Dieffenbacher-Krall, A.C., Almond, P. C., 2013: A revised age for the
1076 Kawakawa/Oruanui tephra, a key marker for the Last Glacial Maximum in New Zealand.
1077 Quaternary Science Reviews, 74, 195-201.

1078 Vermeesch, P., 2010: HelioPlot, and the treatment of overdispersed (U–Th–Sm)/He data. Chemical
1079 Geology, 271(3-4), 108-111.

1080 Vermeesch, P., 2012: On the visualisation of detrital age distributions. Chemical Geology, 312, 190-
1081 194.

1082 Vermeesch, P., 2018: IsoplotR: A free and open toolbox for geochronology. Geoscience Frontiers,
1083 9(5), 1479-1493.

1084 Vucetich, C. T., Pullar, W. A., 1969: Stratigraphy and chronology of late Pleistocene volcanic ash
1085 beds in central North Island, New Zealand. New Zealand Journal of Geology and
1086 Geophysics, 12(4), 784-837.

1087 Vucetich, C. G., Howorth, R. 1976: Late Pleistocene tephrostratigraphy in the Taupo district, New
1088 Zealand. New Zealand Journal of Geology and Geophysics, 19, 51-69.

1089 Wagner, G., Van den Haute, P., 2012: Fission-track dating (Vol. 6). Springer Science & Business
1090 Media.

1091 Wiedenbeck, M. A. P. C., Alle, P., Corfu, F., Griffin, W. L., Meier, M., Oberli, F. V., von Quadt, A.,
1092 Roddick, J.C., Spiegel, W., 1995: Three natural zircon standards for U- Th- Pb, Lu- Hf,
1093 trace element and REE analyses. Geostandards Newsletter, 19(1), 1-23.

1094 Wilson, C.J.N., 2007. The geology of Mayor Island (Tuhua): a brief introduction. Geological Society
1095 of New Zealand Miscellaneous Publication, 123B, 1-26.

1096 Wilson, C. J., Rowland, J. V., 2016: The volcanic, magmatic and tectonic setting of the Taupo
1097 Volcanic Zone, New Zealand, reviewed from a geothermal perspective. Geothermics, 59,
1098 168-187.

1099 Wilson, C. J. N., Houghton, B. F., Lanphere, M. A., Weaver, S. D., 1992: A new radiometric age
 1100 estimate for the Rotoehu Ash from Mayor Island volcano, New Zealand. New Zealand
 1101 Journal of Geology and Geophysics 35, 371-374.

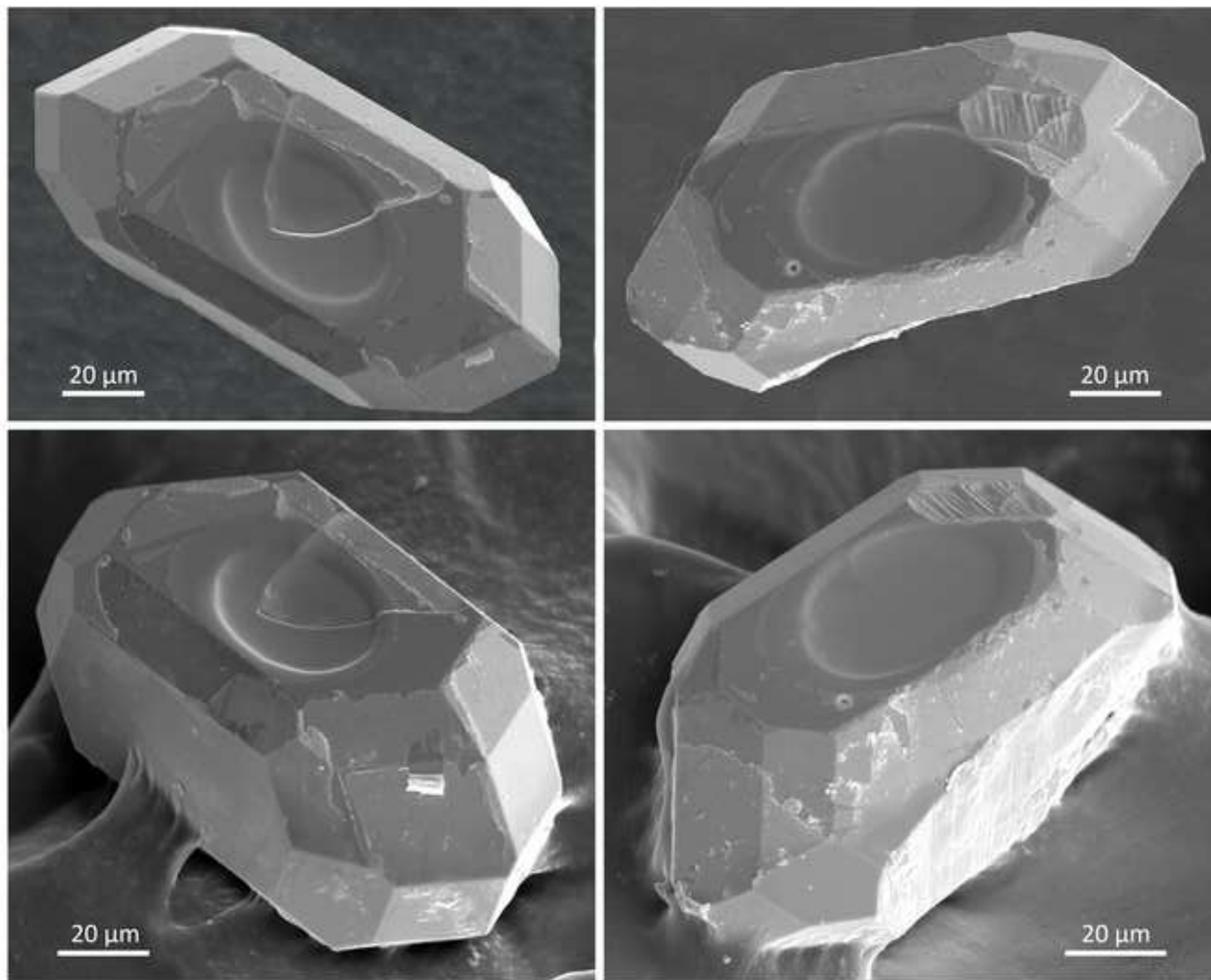
1102 Wilson, C. J. N., Rhoades, D. A., Lanphere, M. A., Calvert, A. T., Houghton, B. F., Weaver, S. D.,
 1103 Cole, J. W., 2007: A multiple-approach radiometric age estimate for the Rotoiti and
 1104 Earthquake Flat eruptions, New Zealand, with implications for the MIS 4/3 boundary.
 1105 Quaternary Science Reviews, 26, 1861-1870.

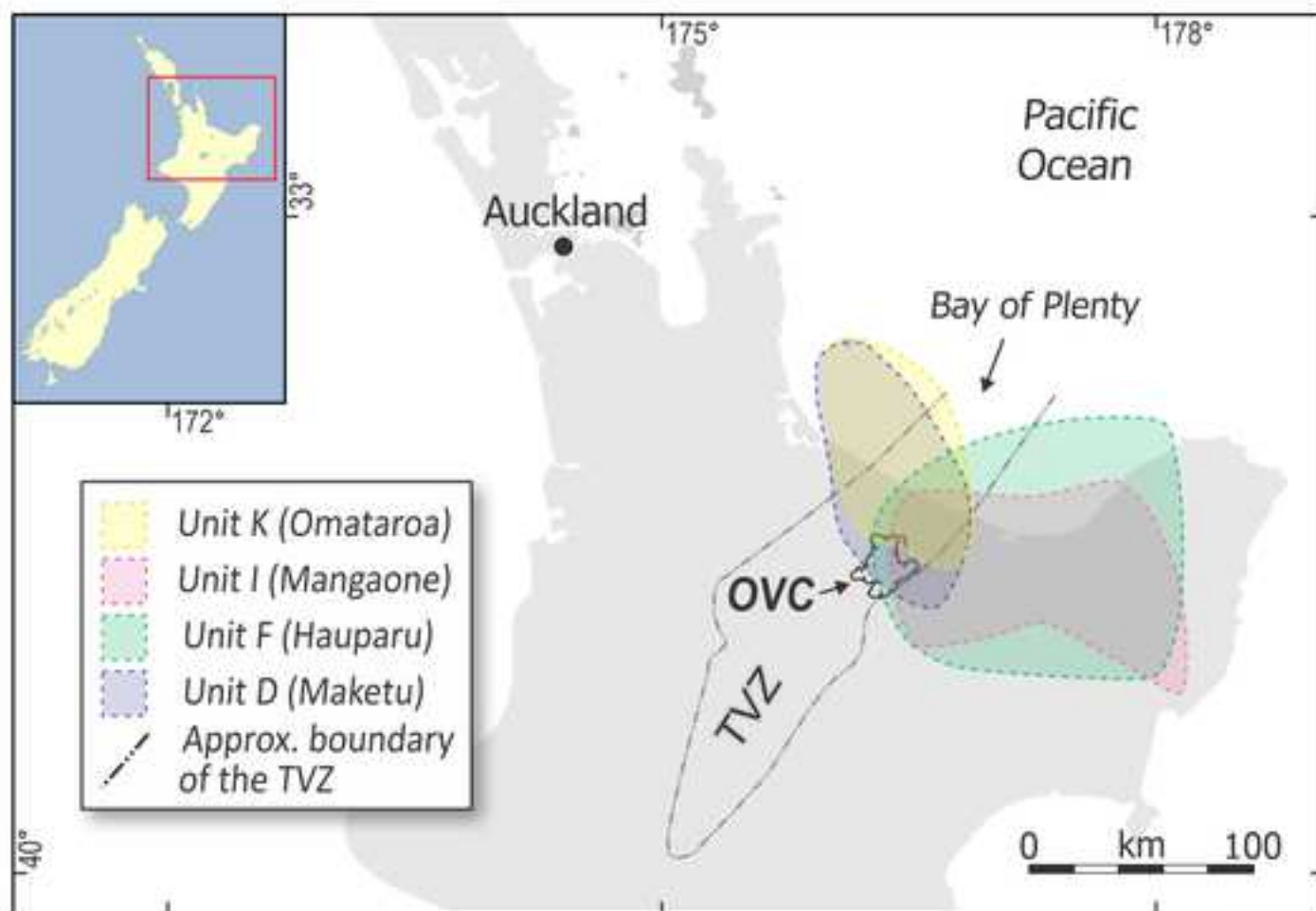
1106 Wilson, C. J. N., Gravley, D. M., Leonard, G. S., Rowland, J. V. 2009. Volcanism in the central
 1107 Taupo Volcanic Zone, New Zealand: tempo, styles and controls. In: Thordarson, T., Self, S.,
 1108 Larsen, G., Rowland, S.K., Hoskuldsson, A. (eds), 'Studies in volcanology: the legacy of
 1109 George Walker'. Special Publications of IAVCEI (Geological Society, London), 2, 225-247.

1110 Wright, I. C., McGlone, M. S., Nelson, C. S., Pillans, B. J., 1995: An integrated latest Quaternary
 1111 (Stage 3 to present) paleoclimatic and paleoceanographic record from offshore northern
 1112 New Zealand. Quaternary Research, 44, 283-293.

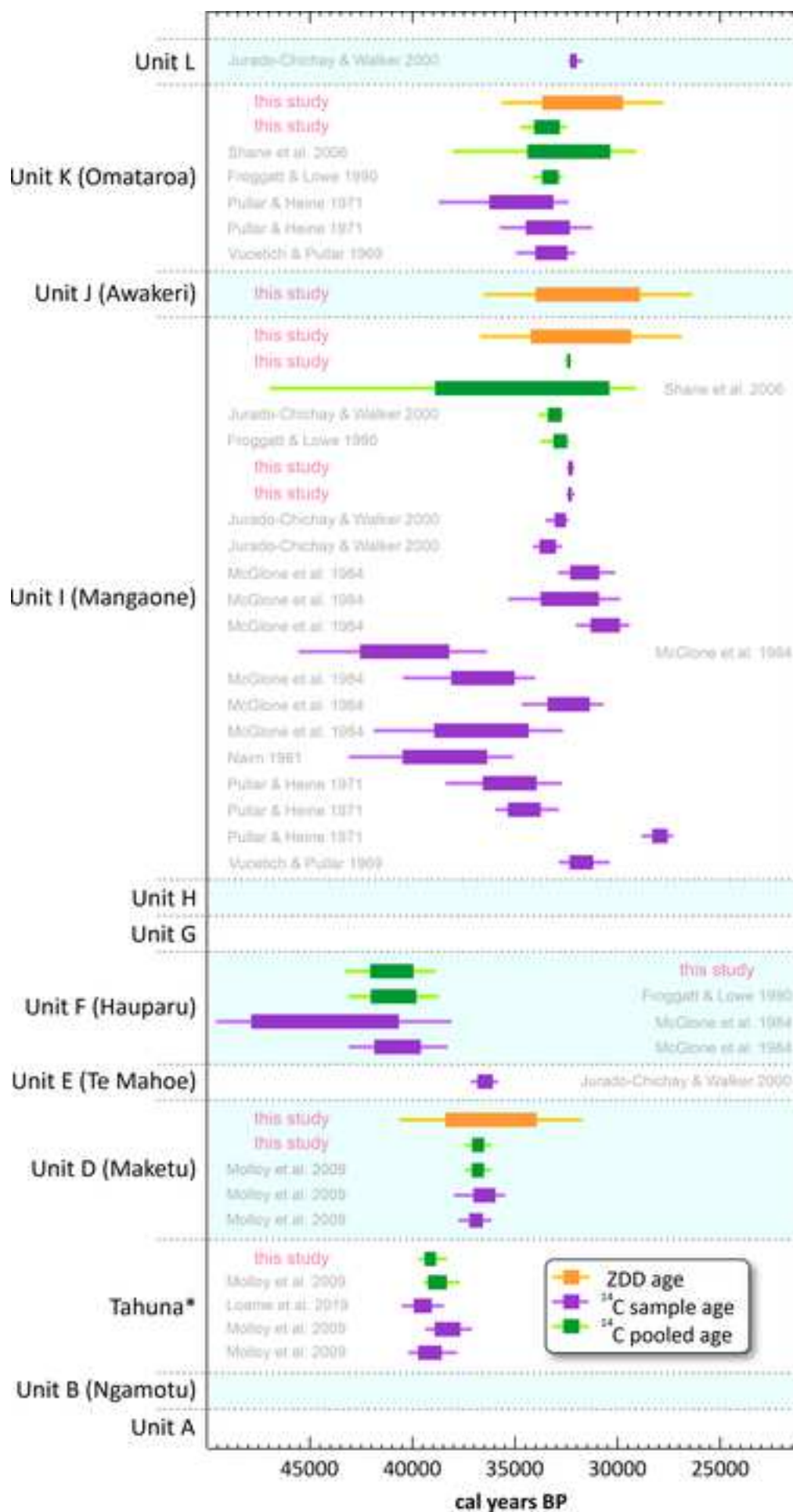
1113

Figure 1





[Click here to access/download;Figure;Figure 3.tif](#) 



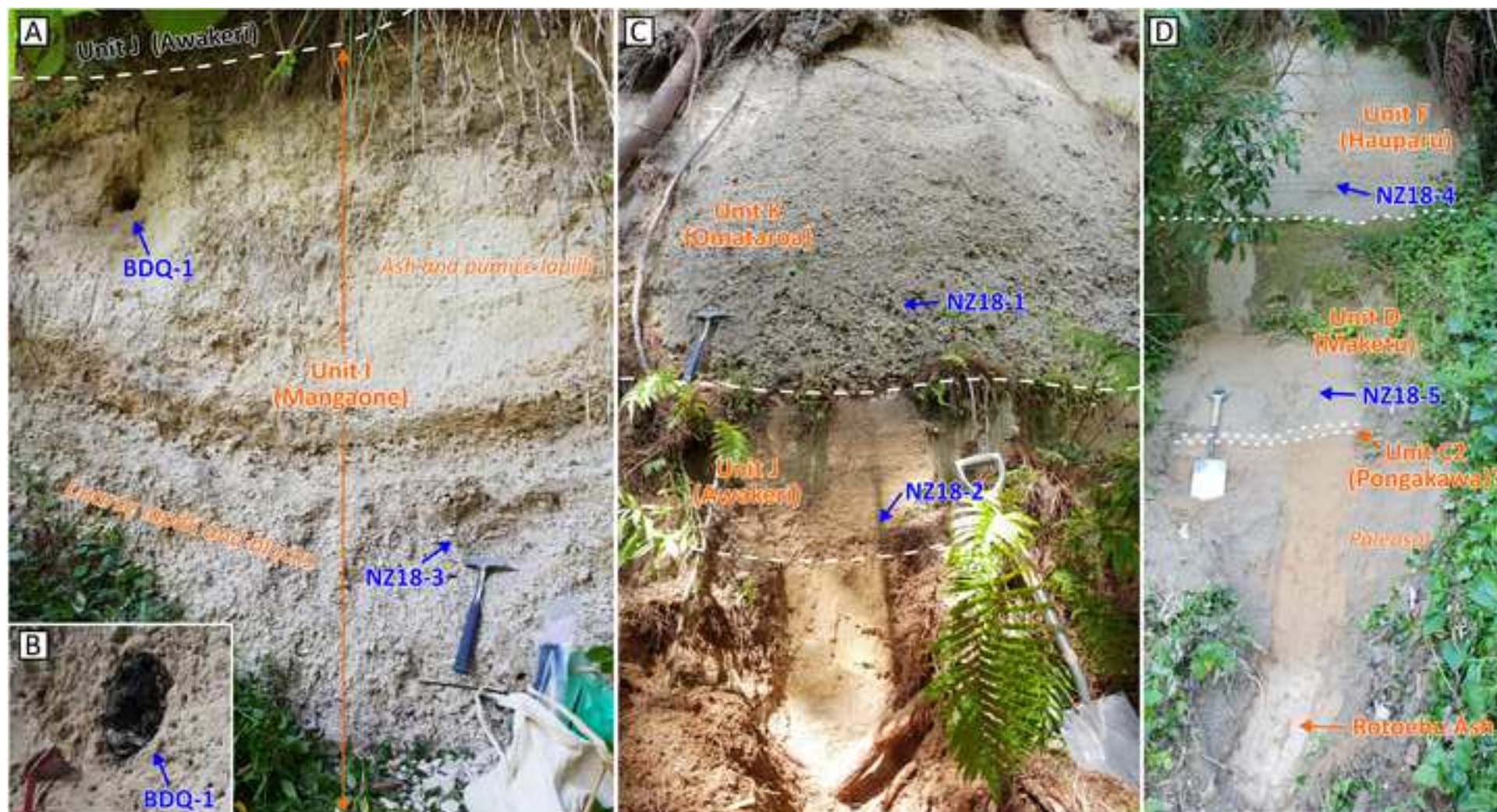


Figure 5

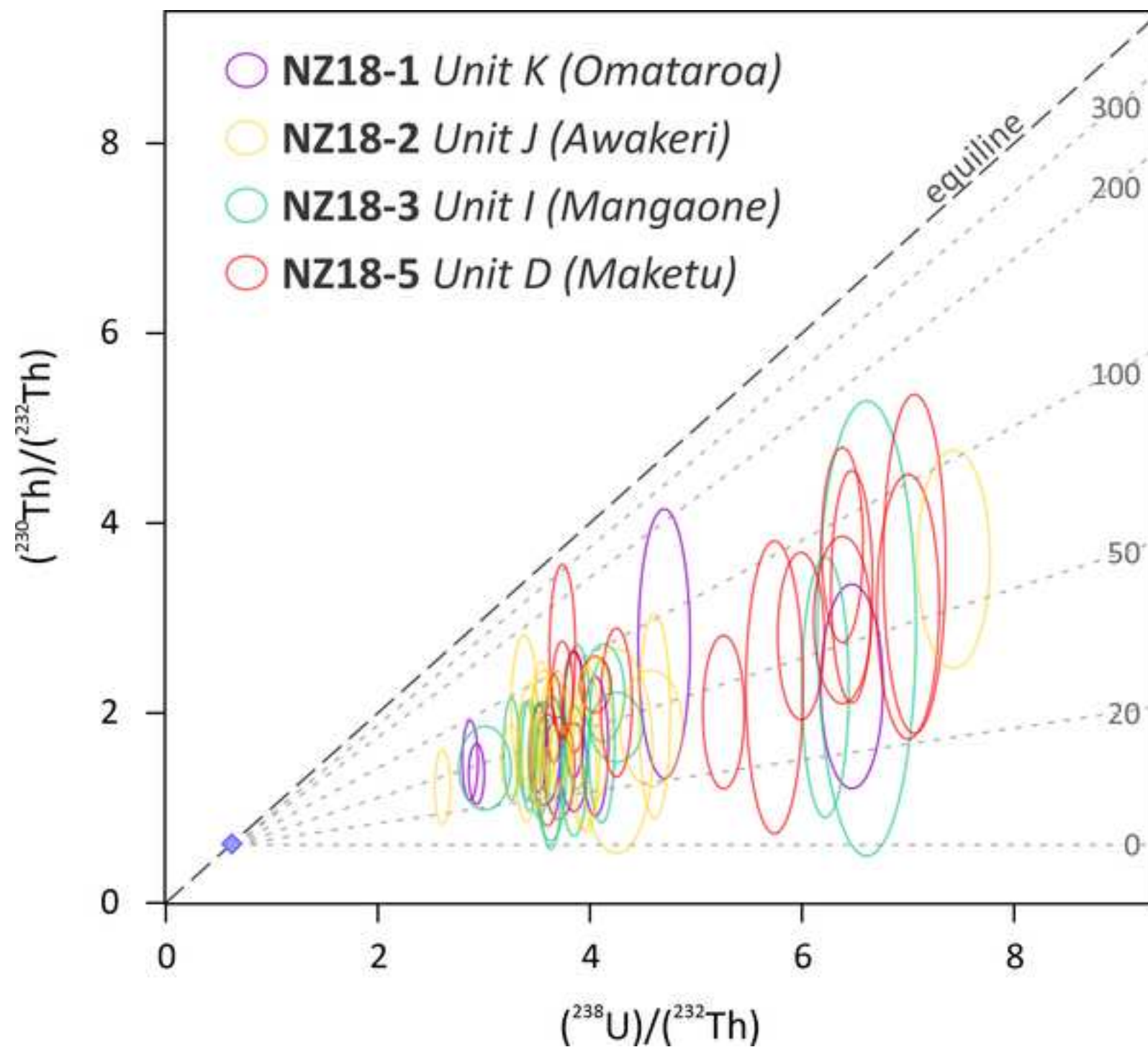
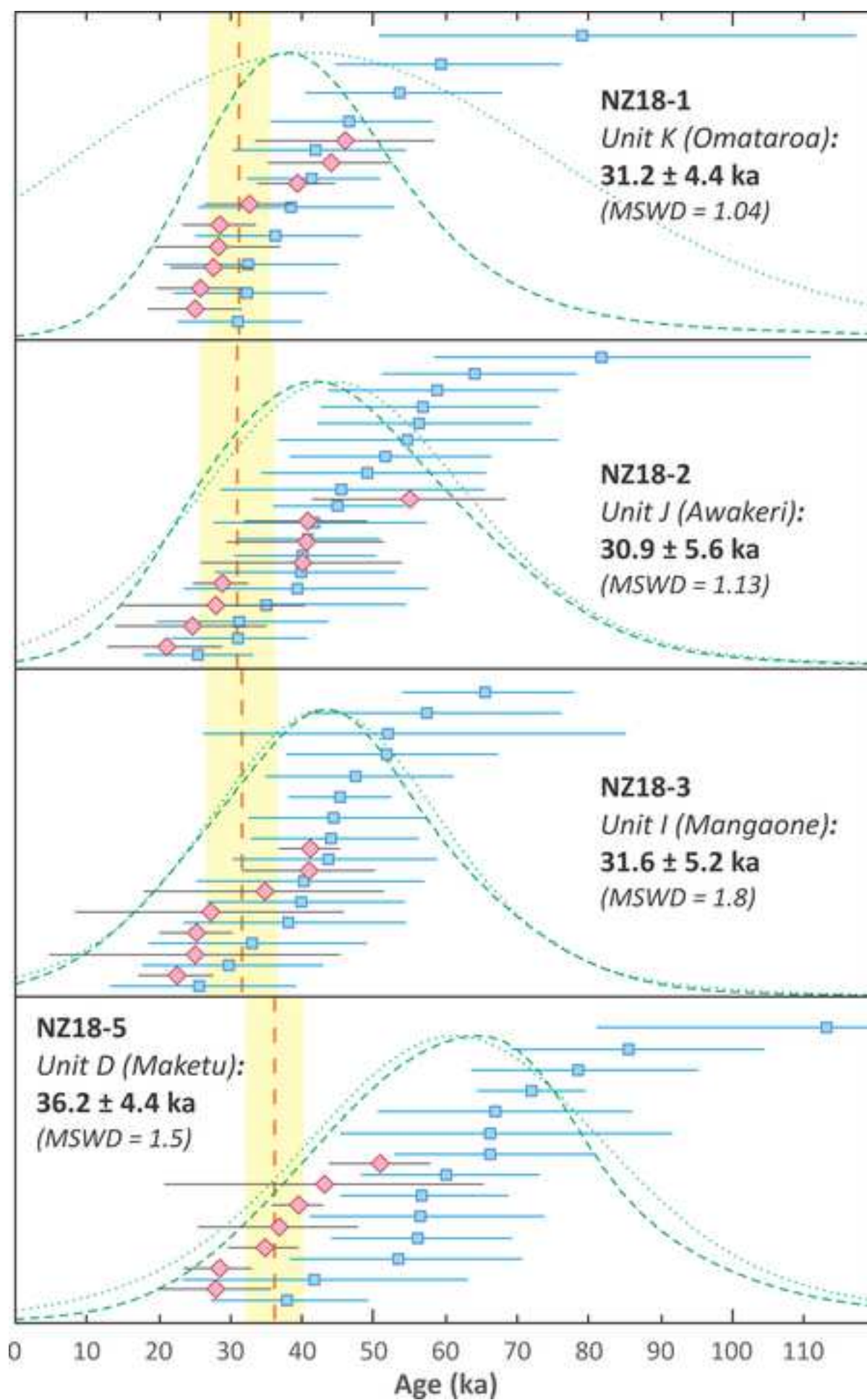
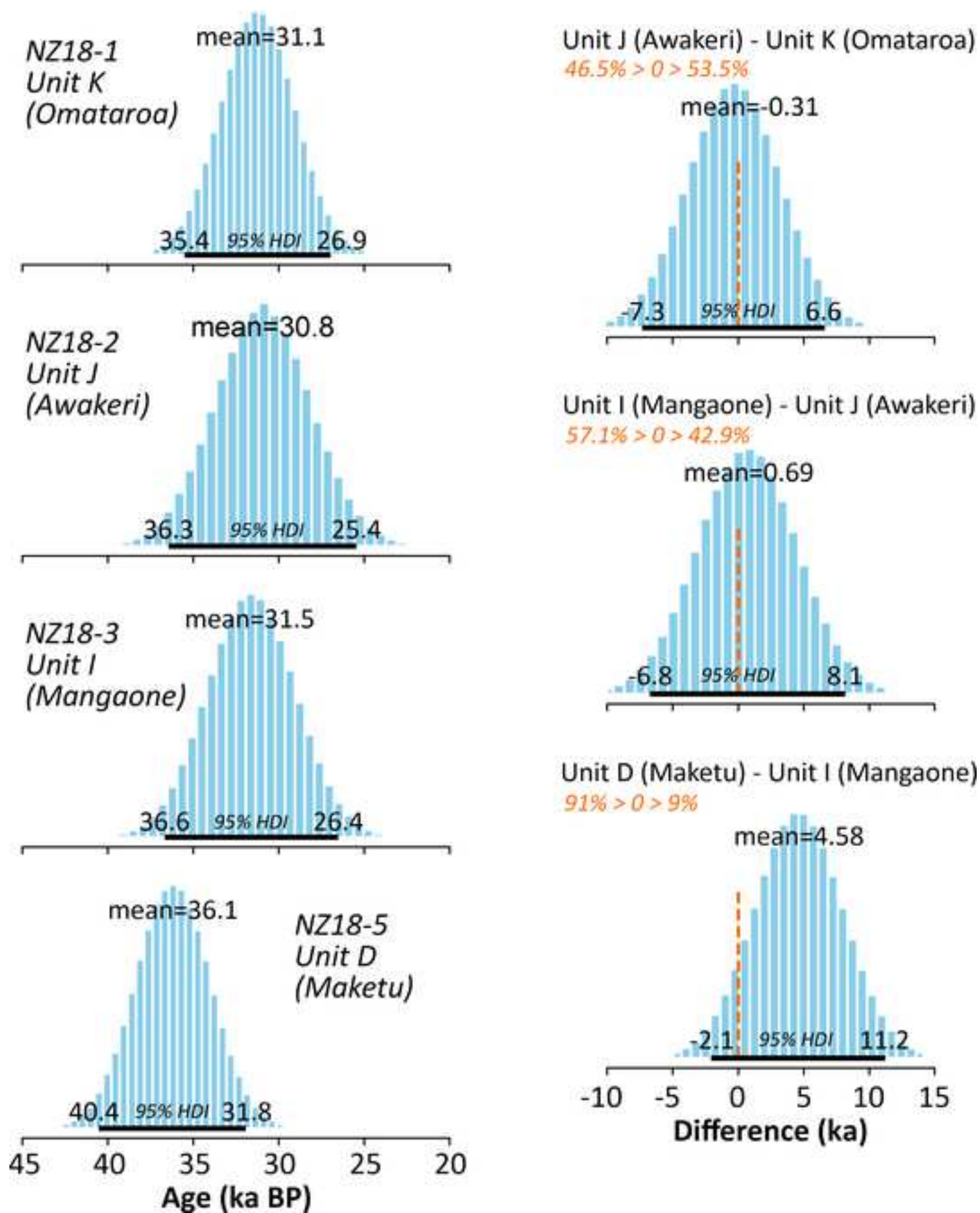
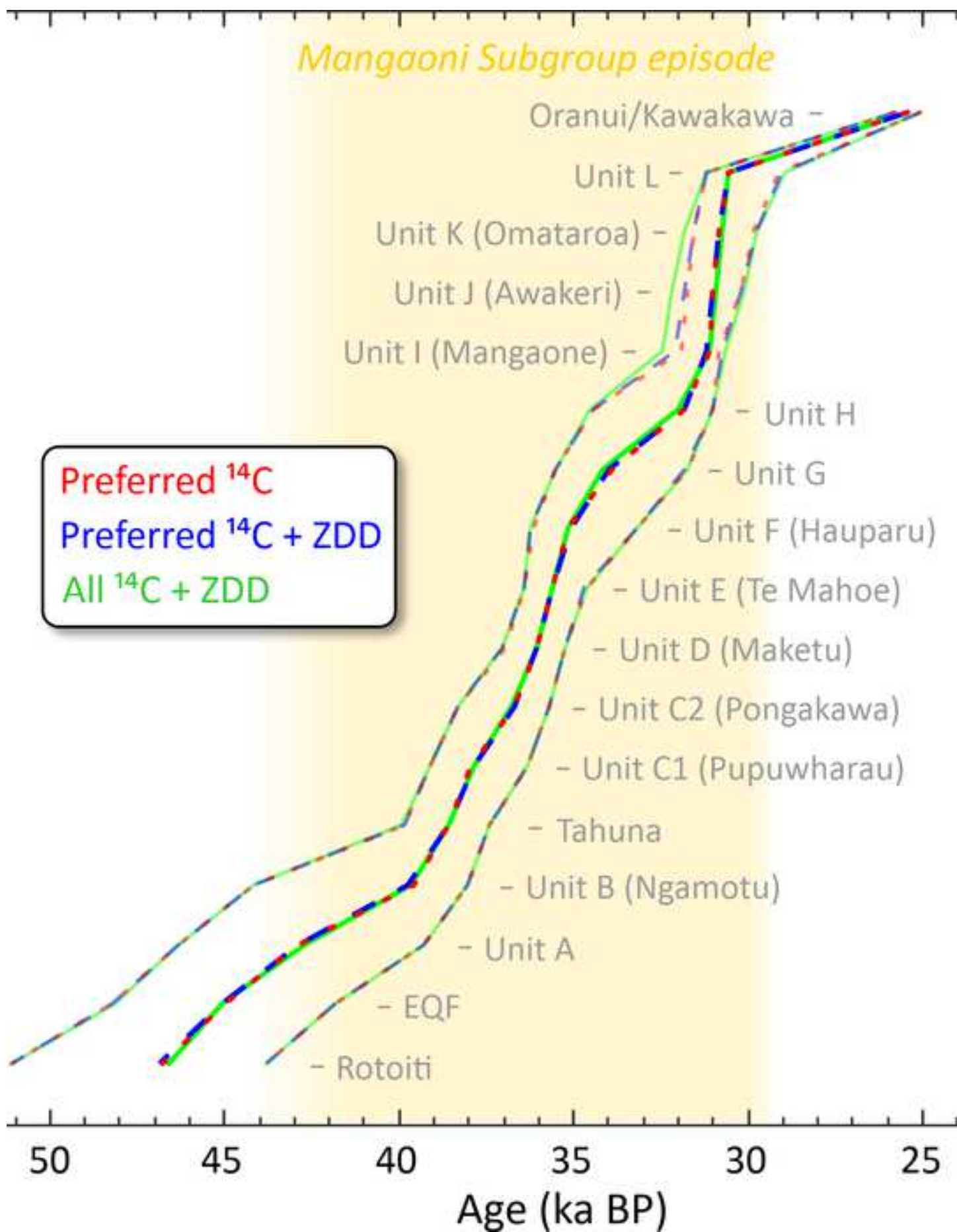
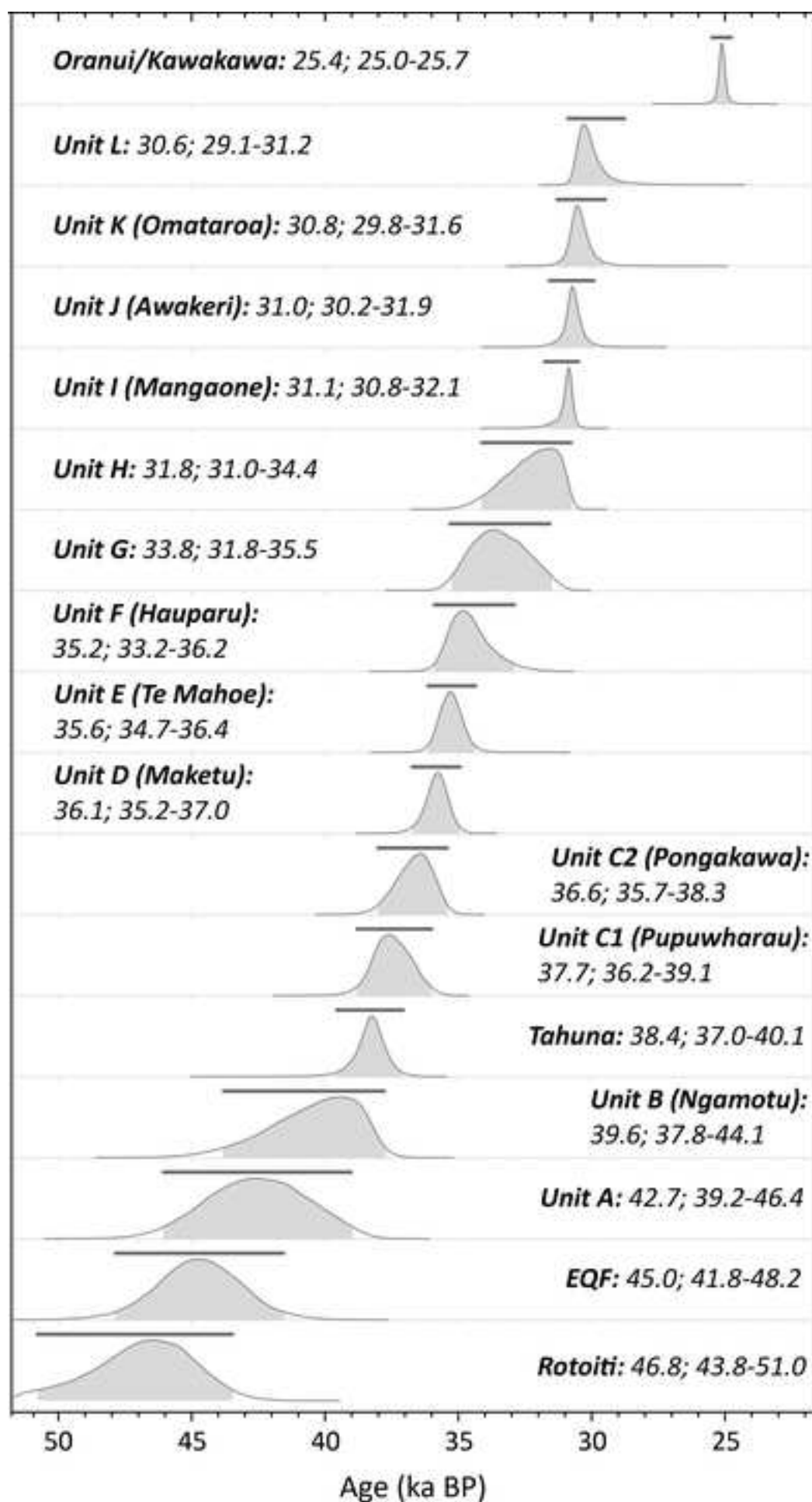


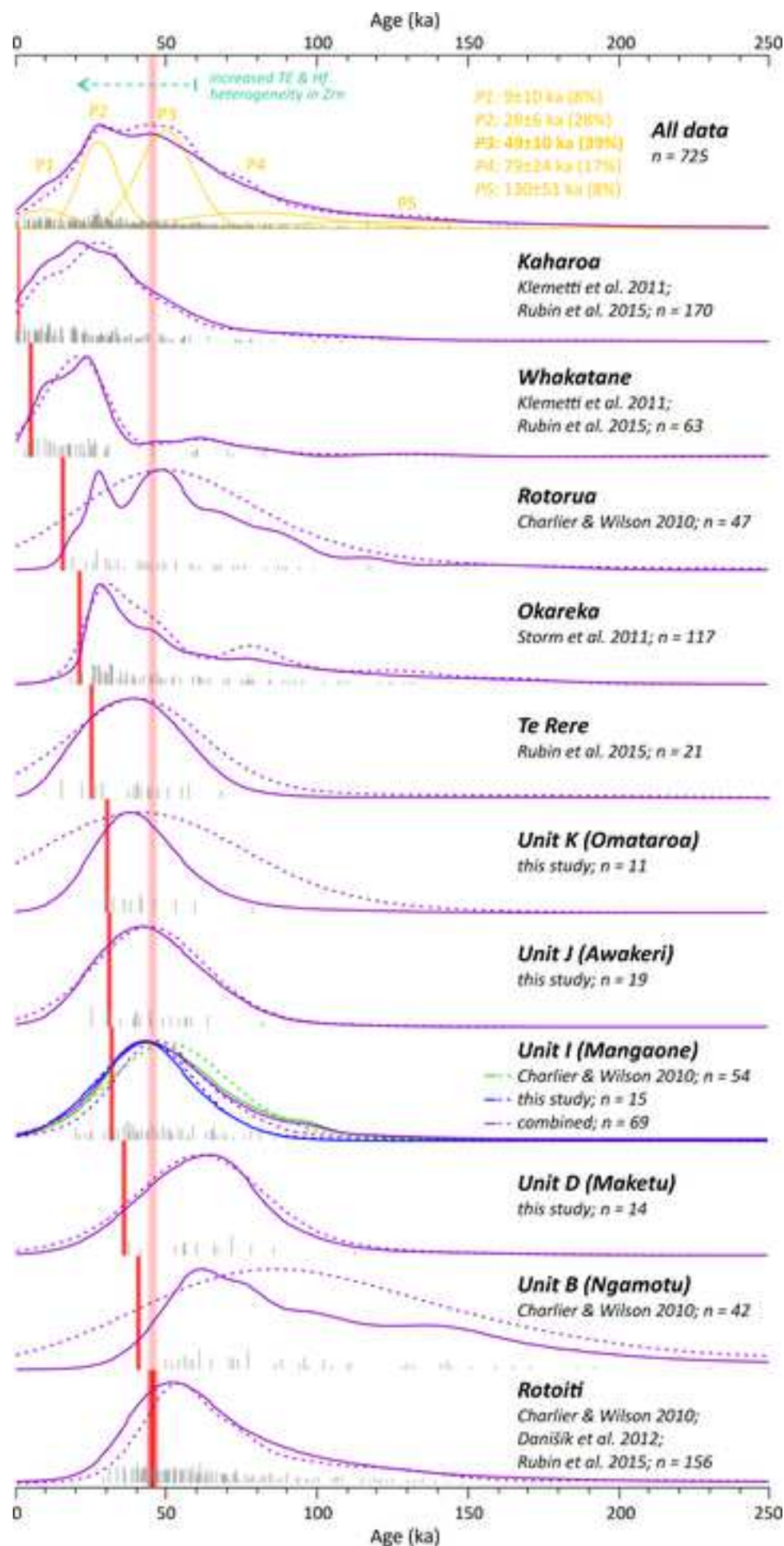
Figure 6

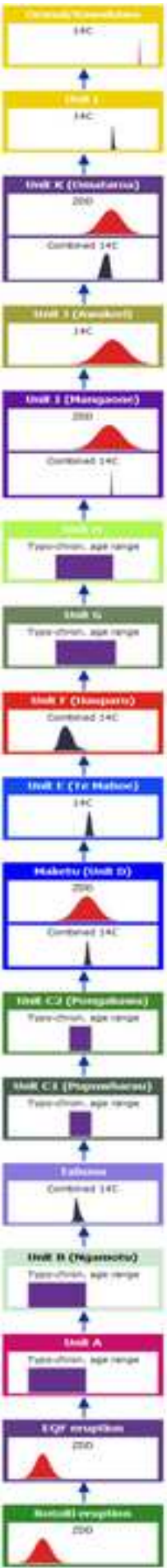
[Click here to access/download;Figure;Figure 6.tif](#)



















[Click here to access/download](#)

Table

[Supplementary Tables_final.xlsx](#)

